1982SSRv...33...17W

PROBING THE SOLAR WIND ACCELERATION REGION USING SPECTROSCOPIC TECHNIQUES*

GEORGE L. WITHBROE, JOHN L. KOHL, and HEINZ WEISER

Harvard-Smithsonian Center for Astrophysics, Cambridge, Mass., U.S.A.

and

RICHARD H. MUNRO

High Altitude Observatory, Boulder, Colo., U.S.A.

Abstract. Measurements of the intensities and profiles of UV and EUV spectral lines can provide a powerful tool for probing the physical conditions in the solar corona out to $8R_\odot$ and beyond. We discuss here how measurements of spectral line radiation in conjunction with measurements of the white light K-corona can provide information on electron, proton and ion temperatures and velocity distribution functions; densities; chemical abundances and mass flow velocities. Because of the fundamental importance of such information, we provide a comprehensive review of the formation of coronal resonance line radiation, with particular emphasis on the H I Lα line, and discuss observational considerations such as requirements for rejection of stray light and effects of emission from the geocorona and interplanetary dust. Finally, we summarize some results of coronal H I Lα and white light observations acquired on sounding rocket flights.

1. Introduction

Improved knowledge of the physical conditions (temperatures, densities and mass flow velocities) in the solar corona is critical to the development of an understanding of the physical state of the corona and the physical mechanisms responsible for coronal heating, solar wind acceleration and the transport of mass, momentum and energy. In this paper we review recent developments in UV and EUV coronagraphic spectroscopy which is becoming a powerful tool for acquiring information on the physical conditions in coronal regions out to 8 solar radii ($R_\odot$) or more from Sun-center. Of particular interest is the solar wind acceleration region beyond $r = 1.5R_\odot$ where present empirical information is extremely limited.

Until recently coronal spectroscopy has been confined primarily to the low corona within a few tenths of a solar radius from the solar surface. At higher levels measurements made through remote sensing techniques have consisted primarily of broad-band measurements of the electron-scattered white light corona, limited observations of forbidden emission lines and limited measurements at radio wavelengths. As a consequence in the solar wind acceleration region for heliocentric distances $r \gtrsim 1.3R_\odot$ there has been very little information on temperatures, flow velocities, the chemical composition and the spatial and temporal variations of these parameters. The available information has been insufficient to place significant empirical constraints upon the identities and functions of:

- plasma heating processes;
- solar wind acceleration processes;

* Paper presented at the IX-th Lindau Workshop 'The Source Region of the Solar Wind'.

Space Science Reviews **33** (1982) 17–52. 0038–6308/82/0331–0017$05.40.
Copyright © 1982 by D. Reidel Publishing Co., Dordrecht, Holland, and Boston, U.S.A.

© Kluwer Academic Publishers • Provided by the NASA Astrophysics Data System

1982SSRv...33...17W

– processes for transport of energy and momentum; and
– processes for producing variations in chemical abundances; or to determine
– the role of different regions in contributing to the outward flow of plasma in the solar wind;
– the dominant physical processes controlling the evolution of transients and the detailed effects of transients on the ambient medium.

This situation is changing rapidly due to the development of coronagraphic techniques employing reflecting optics that permit measurements at large distances above the solar surface in the UV and EUV regions of the spectrum (Kohl *et al.*, 1978, 1981). Access to these spectral regions is important because there are a number of strong permitted coronal lines located there, lines which can provide critical plasma diagnostic information.

Observations of the low corona $r \lesssim 1.3 R_\odot$ acquired with ground-based, rocket and satellite experiments operating in the visible, UV, EUV, and soft X-ray regions of the spectrum have been discussed extensively in the literature and in recent review papers (cf. Withbroe and Noyes, 1977; Vaiana and Rosner, 1978; Zirker, 1981; and references cited therein). We will restrict the present review to the higher layers which, by comparison, have been subjected to only limited spectroscopic probing and therefore offer rich opportunities for empirical investigations. We discuss (1) spectroscopic plasma diagnostic techniques that can be used in the solar wind acceleration region and (2) results of the application of some of these techniques to observations from the Center for Astrophysics/High Altitude Observatory rocket coronagraph program.

2. Coronal Ionization Balance and Particle Velocity Distributions

UV and EUV spectroscopic diagnostics make use of information contained in measurements of the intensities and profiles of spectral lines. These observable parameters depend upon the properties of the plasma emitting the measured radiation. In the upper regions of the corona the densities are sufficiently low that various particle species such as electrons, protons and other ions may have velocity distribution functions characterized by different temperatures. In addition, the ionization balance for a given atomic species may be decoupled from the local electron temperature. One method of illustrating where these effects become important is through comparison of the characteristic time for coronal expansion with the relevant thermalization and ionization equilibrium times. Figure 1 does this for a typical equatorial region (upper graph) and polar region (lower graph). The densities used for these regions are from respectively Saito (1970) and Munro and Mariska (1977), supplemented by values from Allen (1963). The Munro/Mariska model is an updated version of a model by Munro and Jackson (1977) for a large polar coronal hole with rapidly diverging geometry observed during solar minimum in 1973.

For estimating the thermalization times we assumed $T_e = T_p = 2 \times 10^6$ K in the equatorial region and $T_e = T_p = 10^6$ K in the polar region. The expansion times (heavy solid line) $\tau_{\exp} = [(V/n)\, \mathrm{d}n/\mathrm{d}r]^{-1}$ were calculated assuming a particle flux nVA = constant with the area $A \sim r^2$ in the equatorial region and the constant evaluated so as to

© Kluwer Academic Publishers • Provided by the NASA Astrophysics Data System

1982SSRv...33...17W

give a value for the particle flux at 1 AU comparable to that typically observed, 3.8×10^8 protons cm^{-2} s^{-1} (Feldman *et al.*, 1977). For the polar region we used the flow velocities V given by Munro and Mariska who suggested that the outflow in the observed region would be supersonic at low heights ($r \gtrsim 2.3 R_\odot$) *if* the mass flux in polar coronal holes is as large as measured in high speed solar wind streams observed in the ecliptic. The times given in Figure 1 were calculated using H I collisional cross-sections from Percival (1966), hydrogen/proton charge-exchange cross-sections from Fite *et al.* (1962), and the relations for thermalization times given by Spitzer (1962). The ionization equilibrium times for heavy ions vary with the element and stage of ionization. For a representative value we used $\tau_{\text{ions}} = 10^{10}/N_e$ (cf. Bame *et al.*, 1974; Owocki, 1982). The photoionization of H I was determined using measurements of the solar EUV spectrum made using OSO-6 (Dupree *et al.*, 1973) and Skylab (Vernazza and Reeves, 1978).

Because of the long lifetimes of ions in the low density coronal plasma, the ionization balance of heavier elements (e.g. O, Si, Fe) is expected to 'freeze in' within several solar radii of the surface where the lifetimes of the ions become comparable with the coronal expansion time (cf. Hundhausen, 1972; Bame *et al.*, 1974; Owocki, 1982). The ionization equilibrium time for hydrogen $\approx (1/\tau_v + 1/\tau_c)^{-1}$ is much shorter than that of minor ions (see Figure 1), hence the fractional amount of H I freezes in at much greater distances from the Sun. In equatorial regions where the H I collisional ionization times τ_c are much smaller than the corresponding times for photoionization τ_v and coronal expansion (Figure 1a), the ionization balance of H I depends primarily on the electron temperature for $r \lesssim 5 R_\odot$. In low density coronal holes where the H I ionization time may equal or exceed the coronal expansion time at $r \approx 3$ to $4 R_\odot$ (Figure 1b), the H I ionization balance may 'freeze in' within several solar radii of the Sun.

The lifetime of H I atoms $\tau_{\text{H I}} = (1/\tau_c + 1/\tau_v + 1/\tau_{hp})^{-1}$ is much shorter than the coronal expansion time for $r \lesssim 8 R_\odot$ in equatorial regions and $r < 3 R_\odot$ in low density coronal holes. The quantity τ_{hp} is the characteristic time for charge exchange between hydrogen atoms and protons. Thus, in these layers the coupling between the hydrogen atoms and protons is sufficiently strong that the proton and hydrogenic temperatures should be equal. As we shall see in Section 4, this means that the profile of the resonantly scattered H I Lα line can be used to measure proton temperatures in these layers.

Although the neutral hydrogen and proton temperatures are expected to be equal throughout most of the solar wind acceleration region, this is not true for other particles. At $r \gtrsim 2 R_\odot$ the electron/proton thermalization time τ_{ep} is comparable to or larger then the coronal expansion time. Electron/ion thermalization times are also long. Consequently, the temperatures of electrons, protons and ions can differ significantly in this region as shown by theoretical multi-fluid solar wind models (see Hartle and Sturrock, 1968; Nerney and Barnes, 1977; Joselyn and Holzer, 1978; Hollweg, 1978). Thus it is important to develop a technique for distinguishing between the temperatures of different particles species. As shown below, measurements of the profiles of the electron and resonantly scattered components of the coronal Lα line provide a potential means of accomplishing this for electrons and protons. Measurements of spectral lines from heavier ions can provide information on temperatures of other particle species.

© Kluwer Academic Publishers • Provided by the NASA Astrophysics Data System

1982SSRv...33...17W

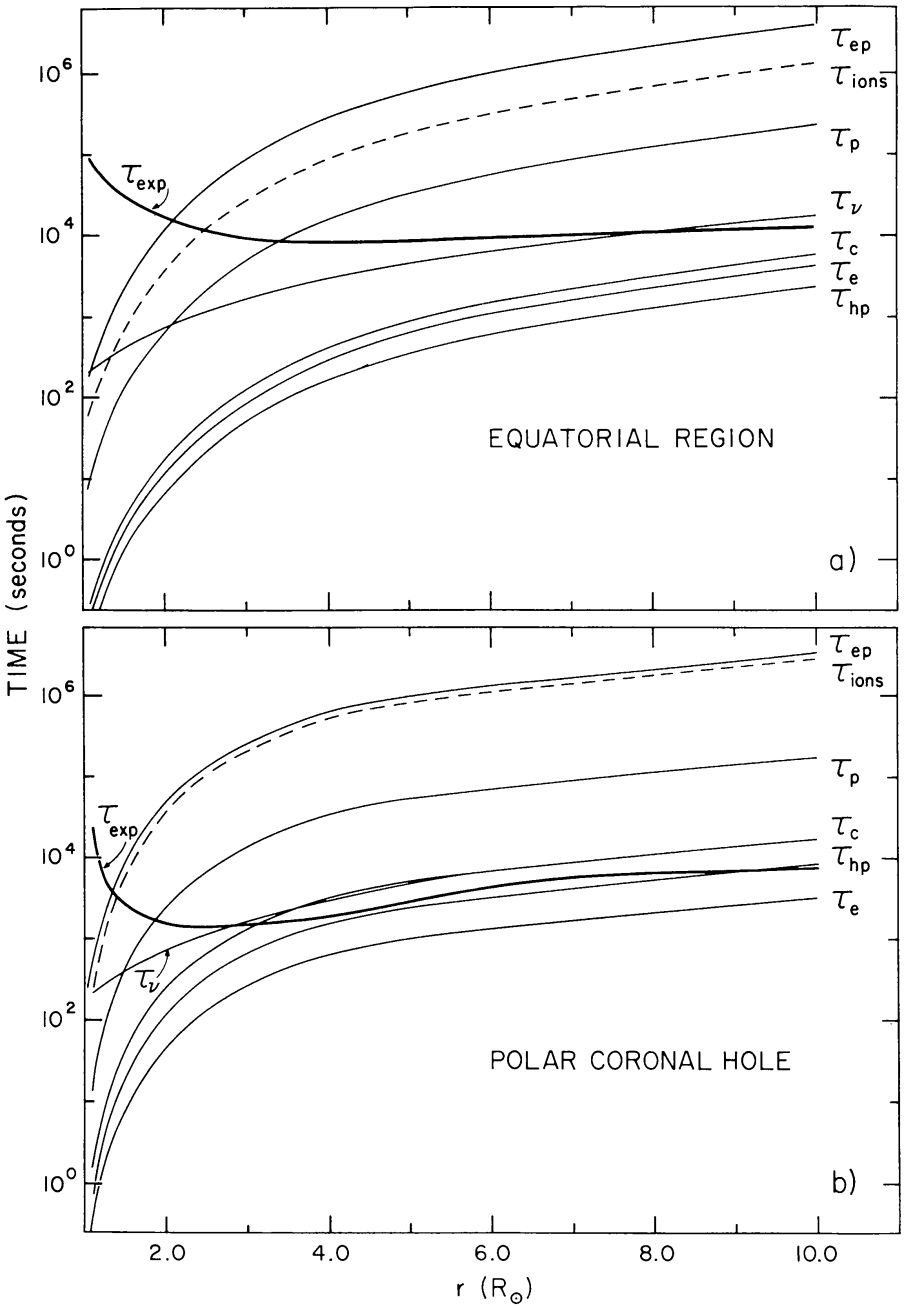

Fig. 1. (a) Characteristic times plotted as a function of heliocentric distance in a typical equatorial region; coronal expansion time τ_{exp}, ionization equilibrium time for typical ions τ_{ions}, H I collisional ionization time τ_c, H I photoionization time τ_ν, electron thermalization time τ_e, proton thermalization time τ_p, time for hydrogen-proton charge exchange τ_{hp} and time for the electron and proton temperatures to equalize τ_{ep}. (b) Same for a low density polar coronal hole.

3. Determinations of Coronal Temperatures and Particle Velocity Distribution

The width of an optically thin spectral line in a low density plasma depends on the kinetic temperature T_{kinetic} of the plasma where the line originates. If the line has a shape which is Gaussian or nearly Gaussian, one can define the kinetic temperature by the relation

© Kluwer Academic Publishers • Provided by the NASA Astrophysics Data System

1982SSRv...33...17W

$$\Delta\lambda_{\mathrm{FWHM}} = \frac{2.4\lambda}{c}\left(\frac{2kT_{\mathrm{kinetic}}}{M}\right)^{1/2}, \tag{1}$$

where T_{kinetic} includes the effect of both thermal and nonthermal motions and M is the mass of the particle species producing the spectral line. The kinetic temperature is a quantity determined directly from the line width. If one wishes to separate the effects of thermal and nonthermal line broadening, then one can define

$$\Delta\lambda_{\mathrm{FWHM}} = \frac{2.4\lambda}{c}\left(\frac{2kT_{\mathrm{thermal}}}{M} + \xi^2\right)^{1/2}, \tag{2}$$

where ξ is the rms velocity component due to plasma motions that occur on a spatial scale much larger than the particle mean free path, but smaller than the path length over which the spectral line is formed. (In the lower solar atmosphere motions of this type are often referred to as microturbulence.) For example, Alfvén waves propagating through the corona (e.g., Hollweg, 1978) may cause plasma motions of sufficient amplitude to significantly broaden spectral lines, perhaps even be the dominant source of broadening for spectral lines of heavy ions. By observing lines from ions of different masses one can obtain empirical constraints on the magnitude of mass-dependent and mass-independent motions. (Line profiles can also be affected by solar wind outflow velocities as will be discussed in Section 4.)

'Temperature' is a convenient parameter, but the line profile gives much more information, namely a direct determination of the velocity distribution of the particles along the line of sight. A static isothermal plasma with a Maxwellian particle velocity distribution produces Gaussian profiles, while a multi-temperature or nonthermal plasma with a non-Maxwellian particle velocity distribution function will yield non-Gaussian profiles. As indicated in Section 2, thermalization times in the solar wind acceleration region are long. As a result, plasma heating, acceleration and/or transport processes that are mass- or charge-to-mass dependent can produce differences in thermal temperatures and/or non-Maxwellian velocity distributions among different species of particles. Consequently, measurements of spectral line profiles can provide constraints on mechanisms for these processes, particularly if measurements of spectral lines from ions of different masses can be acquired.

4. Resonantly Scattered Component of Lα and Determination of T_H and T_p

The H I Lα line provides one of the primary tools for studying the upper corona. There are two components of interest, the resonantly scattered component (FWHM $\approx$ 1 Å) and a much weaker (by about 3 orders of magnitude) electron scattered component (FWHM $\approx$ 50 Å). The resonantly scattered component depends upon the scattering of chromospheric Lα photons by neutral hydrogen atoms in the corona. Even though only about one proton in 10^7 is tied up in neutral hydrogen at coronal temperatures and densities (Gabriel, 1971), the large coronal proton abundance coupled with the high intensity of the chrmospheric Lα radiation gives rise to a coronal resonantly scattered

© Kluwer Academic Publishers • Provided by the NASA Astrophysics Data System

1982SSRv...33...17W

component of Lα strong enough to be measured out to large distances above the solar surface. Resonantly scattered Lα radiation was first observed during the 1970 solar eclipse (Gabriel *et al.*, 1971) and has subsequently been measured by a UV coronagraphic instrument flown on a sounding rocket (Kohl *et al.*, 1980; Weiser *et al.*, 1981). In this section we discuss the formation of this component of Lα. The next section discusses the electron scattered component.

Gabriel (1971) and Beckers and Chipman (1974) have derived equations for the intensity and profile of the resonantly scattered Lα line. The number of coronal hydrogen atoms with velocities between $\mathbf{v}$ and $\mathbf{v} + d\mathbf{v}$ excited per second from level 1 (the ground level) to level 2 (the first excited level) by a beam of chromospheric radiation with wavelengths between λ' and $\lambda' + d\lambda'$ and angular direction between ω and $\omega + d\omega$ is

$$dN_2(\mathbf{v}) = N_1(\mathbf{v}) h B_{12} \lambda_0^{-1} I(\lambda', \omega) \times \\ \times \delta\left(\lambda' - \lambda_0 - \frac{\lambda_0}{c}\,\mathbf{v}\cdot\mathbf{n}'\right) d\omega\, d\lambda'\, d\mathbf{v}, \tag{3}$$

where B_{12} is the Einstein coefficient, h is Planck's constant, and $I(\lambda', \omega)$ is the intensity of the chromospheric radiation at wavelength λ'. The only photons that can be scattered by a hydrogen atom moving with a velocity $\mathbf{v}$ are those with $\lambda' = \lambda_0 + (\lambda_0/c)\mathbf{v}\cdot\mathbf{n}'$ where λ_0 is the central wavelength of the Lα transition and $\mathbf{n}'$ is the vector describing the direction of the incident chromospheric radiation; hence a Dirac delta function has been introduced in Equation (3). (The effect of the natural Lα line width can be ignored for scattering at coronal temperatures.)

The number of photons scattered per second in the direction $\mathbf{n}$ toward an observer is

$$dN = \frac{dN_2(\mathbf{v})}{4\pi}\,\frac{1}{12}\left(11 + 3(\mathbf{n}\cdot\mathbf{n}')^2\right)\delta\left(\lambda_0 - \lambda + \frac{\lambda_0}{c}\,\mathbf{v}\cdot\mathbf{n}\right), \tag{4}$$

where $(11 + 3(\mathbf{n}\cdot\mathbf{n}')^2)/12$ is the angular dependence of the Lα scattering process (see Beckers and Chipman, 1974) and the Dirac delta function transforms the scattered wavelength from the atom's frame to the observer's frame. Now

$$N_1(\mathbf{v})\, d\mathbf{v} = \frac{N_1}{N_{\mathrm{H\,I}}}\,\frac{N_{\mathrm{H\,I}}}{N_p}\,\frac{N_p}{N_e}\,N_e f(\mathbf{v})\, d\mathbf{v} \\ = 0.8 N_e R f(\mathbf{v})\, d\mathbf{v} \tag{5}$$

where $N_1/N_{\mathrm{H\,I}} = 1$ (because of the low coronal density), $R = N_{\mathrm{H\,I}}/N_p$, $N_p/N_e = 0.8$ for a fully ionized plasma with 10% helium and $f(\mathbf{v})$ is the velocity distribution function of the hydrogen atoms.

© Kluwer Academic Publishers • Provided by the NASA Astrophysics Data System

1982SSRv...33...17W

If we employ a rectangular coordinate system with the observer's line of sight being the x-axis, we have

$$I_s(\lambda) = \frac{0.8hB_{12}}{48\pi\lambda_0} \int_{-\infty}^{\infty} N_e R \, dx \int_{\omega} (11 + 3(\mathbf{n}\cdot\mathbf{n})^2) \, d\omega \times$$

$$\times \int_{-\infty}^{\infty} I(\lambda', \omega) \, d\lambda' \int_{-\infty}^{\infty} f(\mathbf{v}) \delta\left(\lambda' - \lambda_0 - \frac{\lambda_0}{c} \mathbf{v}\cdot\mathbf{n}'\right) \times$$

$$\times \delta\left(\lambda_0 - \lambda + \frac{\lambda_0}{c} \mathbf{v}\cdot\mathbf{n}\right) d\mathbf{v}, \qquad (6)$$

where $I_s(\lambda)$ is the intensity of the scattered radiation and $\mathbf{v}\cdot\mathbf{n} = v_x$. If a Maxwellian

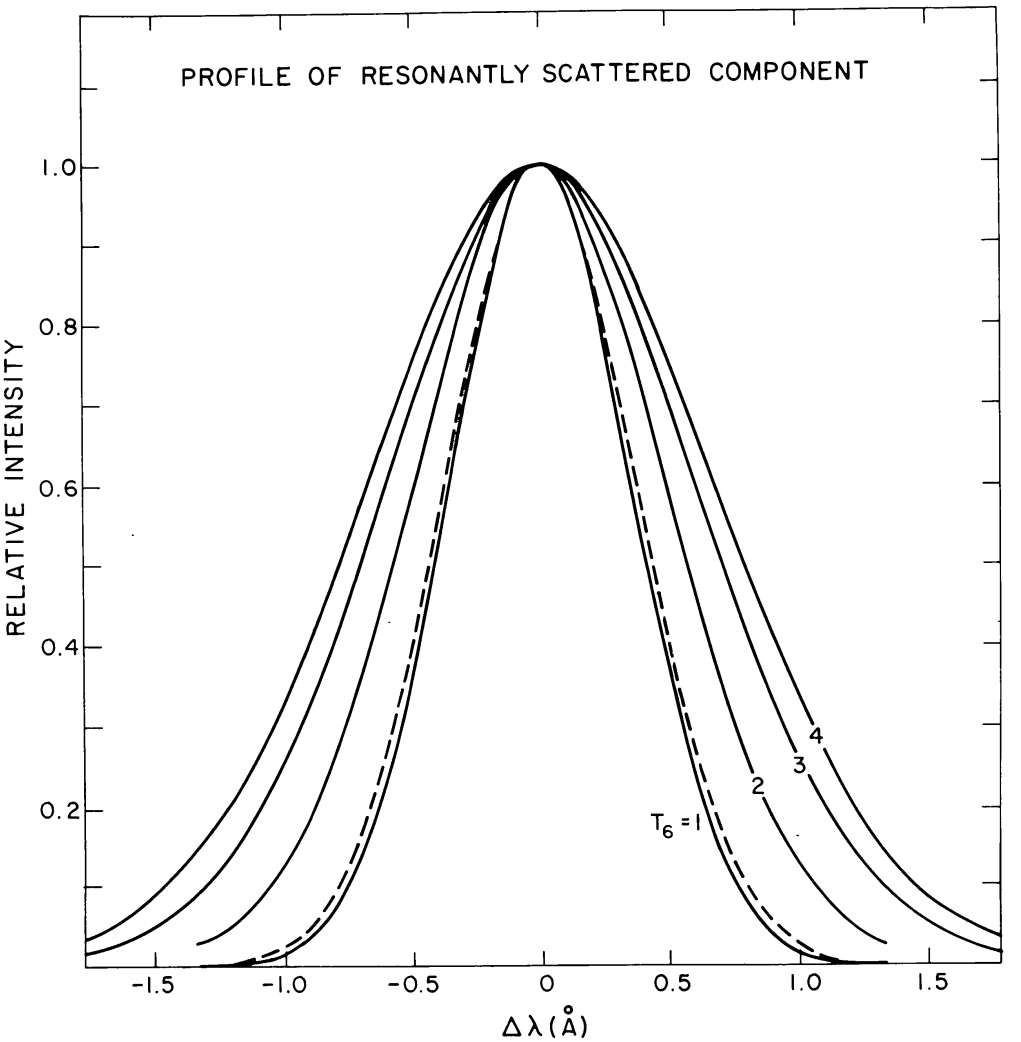

Fig. 2. Profiles of the resonantly scattered component of Lα calculated with a spheric isothermal corona for a line-of-sight intersecting the plane of the solar disk at $\rho = 3R_\odot$ from Sun-center. Profiles for 4 coronal temperatures (in units of 10^6 K) are shown. For comparison a pure Gaussian with a width corresponding to the thermal width is also plotted (dashed line).

© Kluwer Academic Publishers • Provided by the NASA Astrophysics Data System

1982SSRv...33...17W

velocity distribution is assumed, the integral over $\mathbf{v}$ can be integrated analytically to yield an expression for $I_s(v)$ which can then be integrated numerically over x, ω, and λ'.

Figure 2 presents profiles for the resonantly scattered component of Lα for several values of the hydrogen temperature T_H (in units of 10^6 K). These profiles were calculated using an isothermal spherically symmetric corona with a radial density distribution given by Saito (1970). For the profile of the incident chromospheric radiation we used the measurements of Gouttlebroze *et al.* (1978). We assumed that the intensity and shape of the chromospheric profile are constant across the solar disk. The chromospheric Lα line shows little center-limb variation (Prinz, 1974; Basri *et al.*, 1979; and unpublished data from the Harvard Skylab experiment). If the effects of nonthermal motions can be ignored, then the temperatures given in Figure 2 are the hydrogen thermal temperatures T_H. If isotropic nonthermal motions are present which yield a Maxwellian velocity distribution for hydrogen atoms, then the hydrogen temperatures given in Figure 2 correspond to a kinetic temperature $T_k = T_H + \xi^2 m_H/2k$, where ξ is the rms nonthermal velocity. The theoretical resonantly scattered profiles are very nearly Gaussian with widths slightly smaller than that of a Gaussian curve with a Doppler width $\Delta\lambda_0 = (\lambda/c)\sqrt{2kT_H/m_H}$. This is illustrated in Figure 2 by a comparison of the resonantly scattered profile for $T_H = 10^6$ K and the corresponding Gaussian curve (dashed line). The slight differences between the theoretical line profile and the Gaussian curve are due to the details of the scattering process.

Because of the temperature sensitivity of the profile of the resonantly scattered component of Lα, it provides a good diagnostic for determining the coronal hydrogen kinetic temperature. A kinetic temperature is defined here to include the effects of thermal motions, nonthermal motions and outflow of coronal plasma into the solar wind. Corrections for the effects of the outflow are discussed later in this section. If the effects of nonthermal motions and outflows in a given measurement are unknown, then the Lα profile provides an upper limit to the hydrogen thermal temperature. However, since the thermal velocities of hydrogen atoms are very high (160 km s^{-1} for $T_H = 1.5 \times 10^6$ K) compared to nonthermal velocities measured in the low corona, which are of the order of 30 km s^{-1} (e.g. Feldman and Behring, 1974; Moe and Nicolas, 1977), the width of this Lα component is expected to be broadened primarily by thermal motions in the low corona ($r \lesssim 1.3 R_\odot$). At greater distances from Sun-center there are no reliable measurements of nonthermal velocities. However, by measuring widths of spectral lines from heavier ions (e.g. O VI, Mg X, and Fe XII), which are much more sensitive to nonthermal broadening due to their narrow thermal widths, one may be able to place limits on the magnitude of the nonthermal broadening in these higher layers (see Section 6).

The profile of the resonantly scattered component of H I Lα also provides a measurement of the kinetic temperature of protons in regions where the coronal expansion time $\tau_{exp} \gg \tau_{H\,I}$ where $\tau_{H\,I}$ is the lifetime of hydrogen atoms (see Section 2). For most solar regions this means $T_p \approx T_H$ for $r \lesssim 5$ to $10 R_\odot$ (see Figure 1a). In low density coronal holes the solar wind may reach supersonic velocities at low heights. In that case $T_p \approx T_H$ can be assumed only for $r \lesssim 3 R_\odot$ (see Figure 1b). Because of the weak

© Kluwer Academic Publishers • Provided by the NASA Astrophysics Data System

1982SSRv...33..17W

coupling between protons and electrons, the electron temperature may differ significantly from the hydrogen and proton temperatures as indicated in Section 2.

It is important to recognize the advantages of measuring not only the width of the resonantly scattered component, but also its shape, since the shape of the profile contains information on the velocity distribution of the hydrogen atoms (and protons) along the line of sight. In coronal layers more than a few tenths of a solar radius from the solar surface, the thermalization times for protons (and hydrogen atoms) are long as discussed in Section 2. Hence one might expect that solar wind acceleration processes, wave motions and/or coronal heating processes (in particular any which dissipate nonradiative energy by heating protons) may produce non-Maxwellian hydrogen velocity distributions which are directly measurable from the shape of the resonantly component of the Lα profile.

Figure 3 shows how the width of the profile scattered from a plasma element in the line of sight depends on the angle ψ between the vector from Sun-center to the plasma element and the vector defined by the line of sight. Because of the non-negligible effect of the scattering geometry on the profile (particularly for a bright feature such as a streamer far from the plane of the solar disk) the magnitude of the uncertainty in the

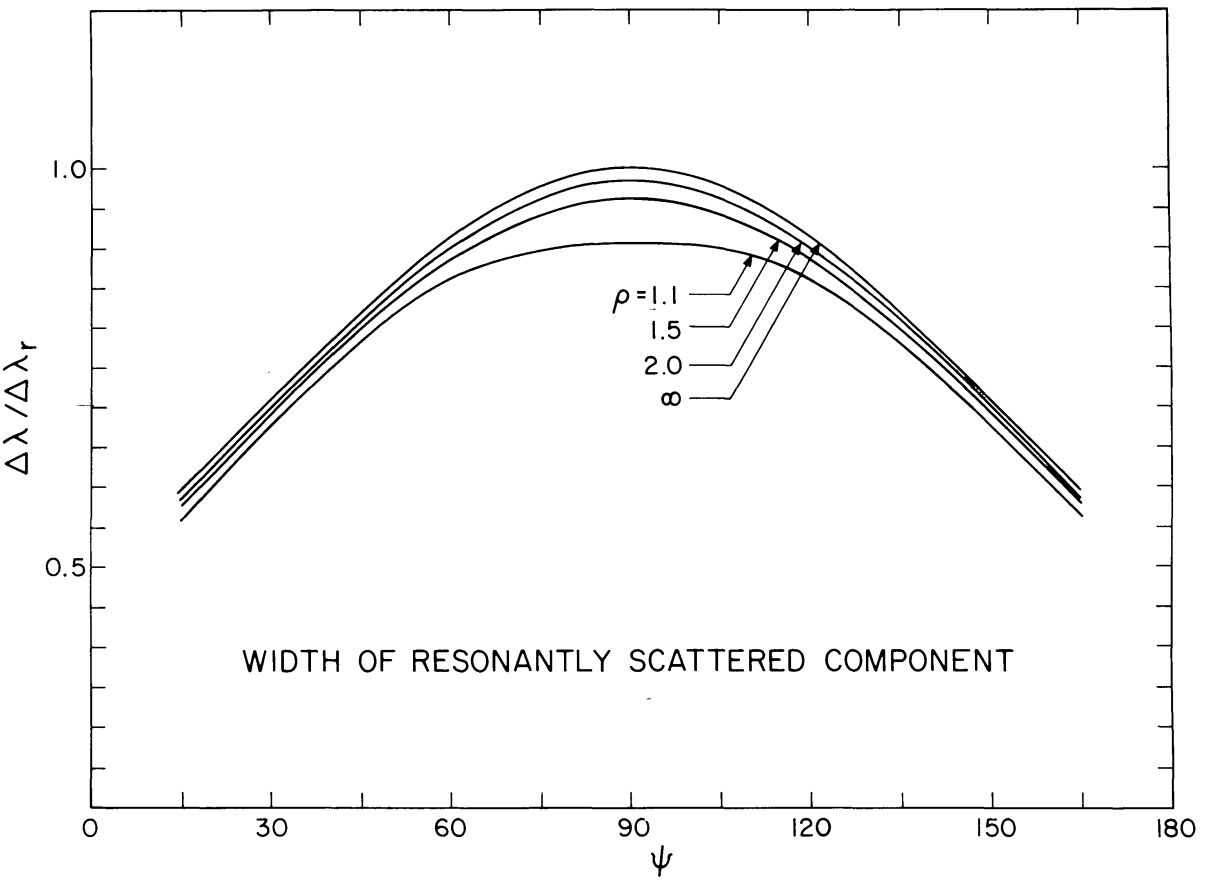

Fig. 3. Width of the resonantly scattered profile from plasma elements at different angular distances ψ where $\psi = 90°$ for a plasma element in the plane of the solar disk. The widths are given in units of the thermal width $\Delta\lambda_r = (\lambda_0/c)\,(2kT_H/m_H)^{1/2}$.

© Kluwer Academic Publishers • Provided by the NASA Astrophysics Data System

1982SSRv...33...17W

temperature (and hydrogen velocity distribution) derived from a measurement of the profile of the resonantly scattered component of Lα will depend on the uncertainty in the geometry assumed in analyzing the measurements. The greater the amount of information that is available concerning the geometry, the lower the uncertainty in the derived temperatures and velocity distribution. Observations of the total intensity and polarization of coronal white light radiation can be used to obtain the required geometrical information for streamers (e.g. Newkirk *et al.*, 1970). For stable features such as coronal holes and many streamers, knowledge of the geometry can be derived from synoptic observations (measurements made periodically over several days) where coronal features can be viewed from different angles as solar rotation carries them around the Sun (e.g. Perry and Altschuler, 1972; Wilson, 1977). Alternatively, or in addition, one can make use of information provided by measurements of features observed on the disk (e.g. He I 10830 observations of coronal holes) or geometries inferred from coronal magnetic field configurations calculated from photospheric magnetograms. For typical observations the uncertainty in T_p resulting from line-of-sight effects should be 10% or less.

There is one additional factor that can affect the profile of the resonantly scattered component of Lα. If one is observing radiation from a region with high mass flow velocities resulting from the outward flow of the solar wind, the profiles can be broadened by the component of the flow velocity in the direction along the line of sight. For example in a radially directed flow there will be a velocity component toward the observer for the plasma on the observer's side of the plane of the solar disk and a component directed away from the observer on the other side of the plane of the solar disk. The Doppler shifts introduced by these components of the solar wind flow will broaden the profile. The amount of broadening will depend on the flow geometry (e.g. radial or nonradial) and speed. For example a radially directed flow which gives constant mass flux in a spherically symmetric isothermal ($T_H = 1.5 \times 10^6$ K) corona with the density gradients used earlier increases the width of a profile observed at $4R_\odot$ by 1.7%, 5.9%, and 12.8% for flow velocities (at $r = 4.0R_\odot$) of 100, 200, and 400 km s^{-1}. However, this effect can be taken into account through use of information on the geometry (determined for example from synoptic data, symmetry arguments) and mass flow velocities derived from Doppler dimming effects (see Section 7 below).

5. Electron Scattered Component of Lα and Determination of T_e

One of the fundamental coronal plasma parameters is the electron temperature. A variety of methods have been used to obtain information on temperatures in the low corona where the densities are high and thermalization times are short. The most commonly used techniques depend upon spectral line ratios. To deduce temperatures from spectral line intensities requires a detailed knowledge of the relevant ionization and excitation processes and in some cases chemical abundances. Ideally, these methods utilize observations of several spectral lines and a large body of atomic data. Such methods are more difficult to apply in the tenuous outer corona; both because of the limited

© Kluwer Academic Publishers • Provided by the NASA Astrophysics Data System

1982SSRv...33...17W

number of observable lines and the uncertainties associated with the long thermalization times. For these reasons, indirect determination of electron temperatures from intensities should not be relied upon, exclusively, for electron temperatures is the solar wind acceleration region, although they do provide some information. Widths of spectral lines from heavy ions are also unreliable indicators of electron temperatures in the solar wind acceleration region due to (1) their sensitivity to broadening by nonthermal or turbulent motions and (2) the reduced collisional coupling between ions and electrons in this atmospheric region which can lead to large differences between electron and ion kinetic temperatures. Temperatures based on radio measurements are affected by uncertainties due to the possible presence of nonthermal sources, optical depth effects, the dispersive, inhomogeneous nature of the coronal plasma, and uncertainties in instrumental calibration. Electron temperatures deduced from electron density gradients are unreliable because of the effects of flows and fact that the electron density gradient depends on the sum of the electron and proton temperatures whose relative values are unknown.

Cram (1976) has advocated use of the shape of the electron scattered photospheric spectrum near 4000 Å as an electron temperature diagnostic. However, the requirements on photospheric precision are extremely tight. The uncertainty in coronal temperature corresponding to $\pm 1\%$ accuracy in the ratio of the intensities at 4100 and 3900 Å is $\pm 0.2 \times 10^6$ K. The problem of rejecting stray light in the visible and separating the contributions of the *K*-corona (electron scattered corona) and *F*-corona (dust scattered corona) pose additional difficulties. Corrections for scattering geometry for this method, which are similar to those required for temperature measurements based on electron scattered H I Lα, are discussed later in this section. Given the above considerations it is useful to consider a means of directly measuring coronal electron temperatures, a method that depends upon measurements of the electron scattered component of H I Lα. This means of measuring coronal temperatures was first suggested by Hughes (1965).

The electron scattered component of the coronal Lα radiation is produced by Thomson scattering of chromospheric Lα emission. The problem of determining the scattering of monochromatic radiation by coronal electrons has been addressed by van Houten (1950) and others concerned with the scattering of the photospheric white light spectrum. Consider the scattering of a beam of chromospheric Lα radiation with intensity $I(\lambda', \omega)$, wavelength between λ' and $\lambda' + d\lambda'$ and angular direction between ω and $\omega + d\omega$. The number of incident Lα photons $cm^{-3}\ s^{-1}$ scattered by coronal electrons with velocities between v_e and $v_e + dv_e$ is

$$dN = N_e(v_e)\sigma I(\lambda', \omega)\, d\lambda'\, d\omega\, dv_e\,, \tag{7}$$

where σ is the Thomson scattering cross-section. The fraction of these photons scattered toward an observer is

$$dN(\lambda) = \frac{dN}{4\pi}\frac{3}{4}(1 + (\mathbf{n}\cdot\mathbf{n}')^2)\delta\left[\left(\lambda' - \frac{\lambda'}{c}\,\mathbf{v}_e\cdot\mathbf{n}'\right) - \left(\lambda - \frac{\lambda}{c}\,\mathbf{v}_e\cdot\mathbf{n}\right)\right], \tag{8}$$

© Kluwer Academic Publishers • Provided by the NASA Astrophysics Data System

1982SSRv...33...17W

where $3((1 + (\mathbf{n} \cdot \mathbf{n}')^2)/4$ is the angular dependence of Thomson scattering and $\mathbf{n}'$ and $\mathbf{n}$ are the directions of the incident and scattered photons. Since these photons must have the same wavelength in the rest frame of the electrons, the Dirac delta function specifies which incident photons will be scattered at wavelength λ measured by the observer. Hence the intensity (photons $\mathrm{cm}^{-2}\,\mathrm{s}^{-1}\,\mathrm{sterad}^{-1}$) of the electron scattered component of Lα is given by

$$I_e(\lambda) = \frac{3\sigma}{16\pi} \int_0^\infty N_e \, dx \int_\omega d\omega (1 + (\mathbf{n}' \cdot \mathbf{n})^2) \int_{-\infty}^{\infty} I(\lambda', \omega) \, d\lambda' \times$$

$$\times \int_{-\infty}^{\infty} f(\mathbf{v}_e) \delta \left[\left(\lambda' - \frac{\lambda'}{c} \mathbf{v}_e \cdot \mathbf{n}' \right) - \left(\lambda - \frac{\lambda}{c} \mathbf{v}_e \cdot \mathbf{n} \right) \right] d\mathbf{v}_e , \qquad (9)$$

where x is the distance from the observer along the line of sight. Because of the high thermal velocity of electrons at coronal temperatures, nearly 7000 km s^{-1} for $T_e = 1.5 \times 10^6$ K, we will neglect the effects of solar wind flows and turbulence on the

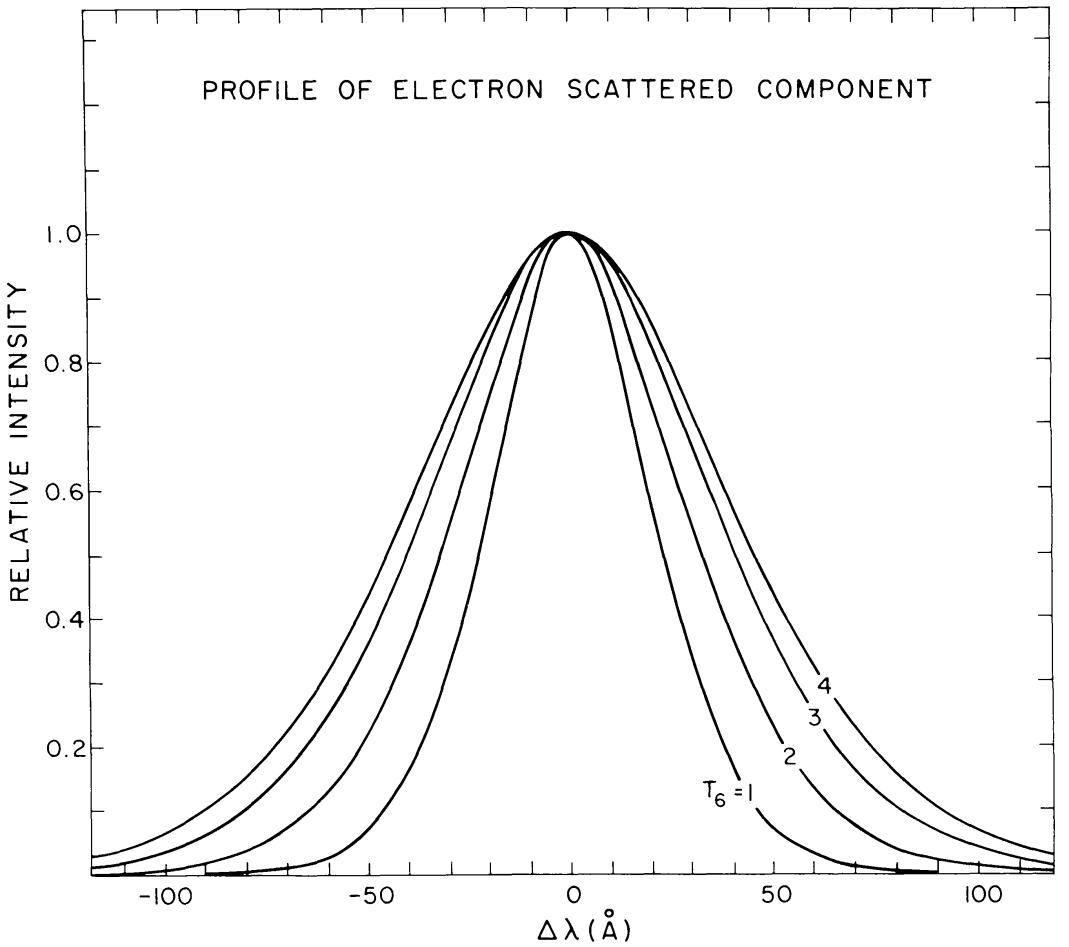

Fig. 4. Profiles of the electron scattered component of Lα calculated with a spherically symmetric isothermal corona for $\rho = 3$. Profiles for 4 coronal temperatures (in units of 10^6 K) are shown.

© Kluwer Academic Publishers • Provided by the NASA Astrophysics Data System

1982SSRv...33...17W

electron velocity distribution. If one further assumes that the coronal electrons have a Maxwellian velocity distribution, one can integrate over $\mathbf{v}_e$ analytically and obtain an expression for the scattered radiation which can be numerically integrated over x, ω, and λ'.

Figure 4 contains plots of profiles for the electron scattered component of coronal Lα radiation computed using Equation (9) for a spherically symmetric isothermal corona with the same radial density distribution used above for calculating resonantly scattered profiles. These profiles show the sensitivity of the width of the electron scattered component to the magnitude of the coronal electron temperature. Due to the low mass of the scattering particles, the width of this component is much larger than the resonantly scattered component of Lα. The sensitivity of the profile of the electron scattered component to variations in the coronal electron temperature means that it can provide a method for spectroscopic determination of this critical coronal parameter. It is particularly important to note that not only can one obtain information on the electron temperature, but also information on the velocity distribution of the electrons along the line of sight (which determines the shape of the profile). As shown in Figure 1 electron thermalization times in the corona increase rapidly with height. Consequently, solar wind acceleration processes or nonthermal processes which heat the coronal electrons may produce departures from a Maxwellian velocity distribution that are detectable as distortions in the shape of the electron scattered Lα profile.

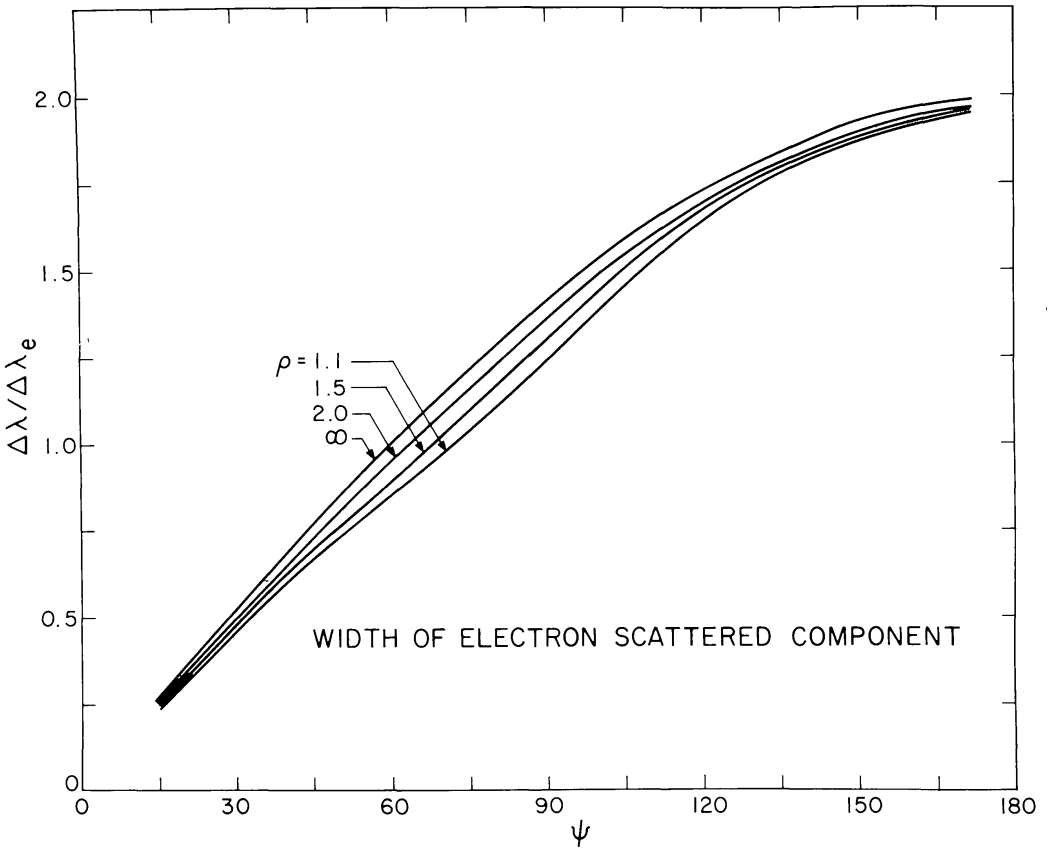

Fig. 5. Width of the electron scattered profile for plasma elements at different angular distances ψ where $\psi = 90°$ for a plasma element in the plane of the solar disk. The widths are given in units of the thermal width $\Delta\lambda_e = (\lambda_0/c)\,(2kT_e/m_e)^{1/2}$.

© Kluwer Academic Publishers • Provided by the NASA Astrophysics Data System

1982SSRv...33...17W

It is important to note that the shape of the electron scattered component of Lα depends on the scattering geometry and is not simply a Gaussian with a Doppler width $\Delta\lambda_0 = (\lambda_0/c)\sqrt{2kT_e/m_e}$. The width $\Delta\lambda_e$ of the scattered radiation from a coronal plasma element depends on the angle ψ between the vector from Sun-center to the plasma element and the vector defined by the line of sight. One can show that $\Delta\lambda_e \approx 2\Delta\lambda_0 \sin(\psi/2)$ (van Houten, 1950). For a plasma element in the plane of the solar disk ($\psi = 90°$) the profile is Gaussian with a characteristic width that is a factor of $\sqrt{2}$ larger than the Doppler width. For plasma elements on the observer's side of the plane of the disk the width $\Delta\lambda_e$ decreases (as $\sin\psi/2$) with increasing angular distance (measured from Sun-center) from the plane of the disk, while on the opposite side the width increases with increasing angular distance. This is illustrated in Figure 5 which presents curves showing the variation of the width of profiles from plasma elements at different angular distances ψ from the plane of the disk. Curves (calculated with Equation (9)) are plotted for several values of ρ where ρ is the distance in solar radii from

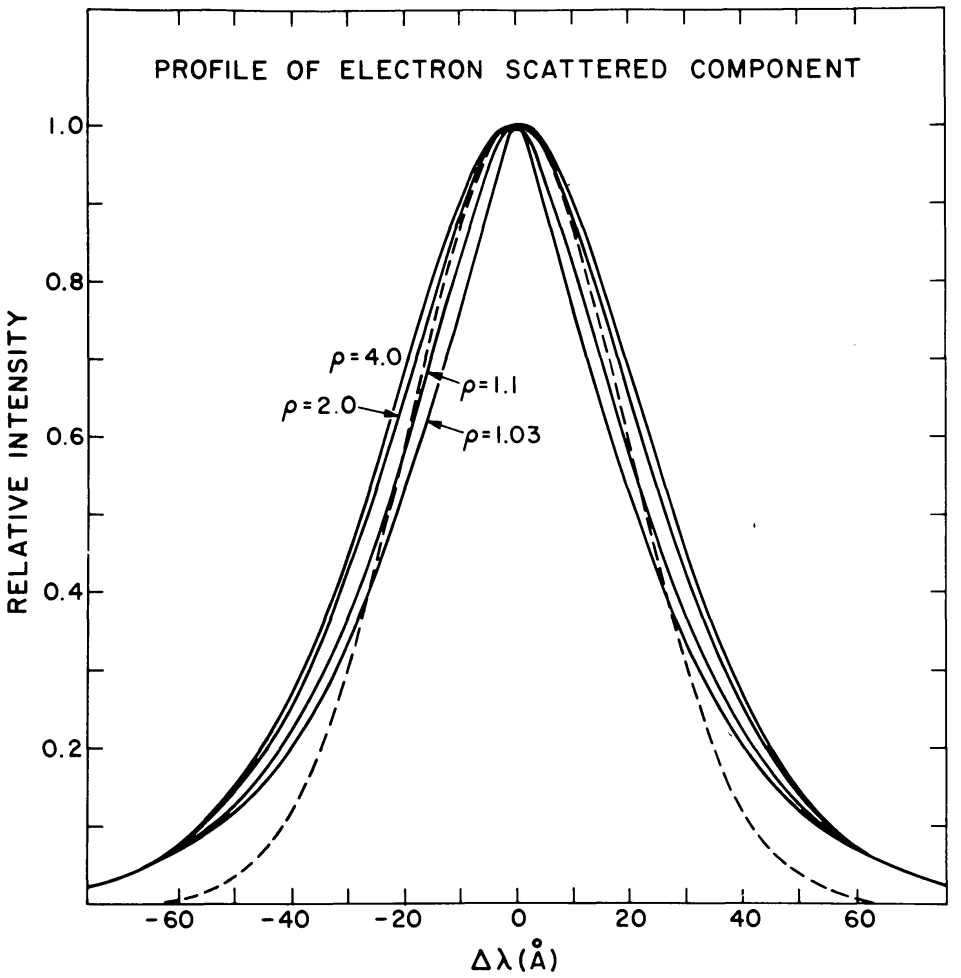

Fig. 6. Profiles (solid lines) of the electron scattered component of Lα calculated for several values of ρ (units of $R_\odot$) using an isothermal coronal model with $T_e = 1.5 \times 10^6$ K. For comparison a pure Gaussian curve with a width corresponding to the thermal width is also plotted (dashed line).

© Kluwer Academic Publishers • Provided by the NASA Astrophysics Data System

1982SSRv...33...17W

Sun-center to the point where the observer's line-of-sight intersects the plane of the solar disk. For large values of ρ where the angular size of the solar disk is small (as viewed from the corona), these curves approach the value $\Delta\lambda_e = 2\Delta\lambda_0 \sin(\psi/2)$.

Figure 6 illustrates the effect of the above ψ dependence on the shape of the profile of the electron scattered Lα line. Theoretical profiles for an isothermal corona with $T_e = 1.5 \times 10^6$ K are given for several values of ρ. The profiles have been normalized to have the same central intensity. The dashed line is a Gaussian curve with a width corresponding to the thermal width $\Delta\lambda = 27.3$ Å $= (\lambda_0/c)\sqrt{2kT_e/m_e}$. The change in shape of the profile with ρ is caused by the decrease (with increasing ρ) of the angular size of the solar disk (as viewed from the coronal plasma elements scattering the radiation) as well as by the decreasing density gradient which determines the distance along the line of sight over which the coronal plasma makes a significant contribution to the total scattered radiation. Note that for $\rho \gtrsim 1.1$, the theoretical profiles are broader (FWHM) than the Gaussian curve. For large values of ρ ($\gtrsim 5R_\odot$) the width of the scattered line is a factor of $\sqrt{2}$ larger than the width of a Gaussian profile with a thermal width $\Delta\lambda_0 = (\lambda_0/c)\sqrt{2kT_e/m_e}$. The L$\alpha$ profiles calculated by Hughes (1965) appear to be too narrow by a factor of approximately 1.4, perhaps due to the neglect of this factor of $\sqrt{2}$.

Since the intensity of the scattered radiation measured at a given position is an integral over the contributions of plasma elements distributed along the line of sight, one cannot simply fit a Gaussian curve to a measured profile and determine the electron temperature from the width. One must account for the geometry of the features in the line of sight (see Section 4). This can be accomplished by modeling techniques. For typical observations the uncertainty in T_e resulting from uncertainties in the geometry should be less than 25%. This source of uncertainty occurs for any electron scattered spectral feature whose shape is used to determine electron temperatures.

6. Determination of T_i from Spectral Line Profiles of Ions

Although much information can be derived from the H I Lα line, a much more complete description is obtained when other UV and EUV spectral lines are also observed. There are a number of UV and EUV ($\lambda > 500$ Å) spectral lines (e.g. from C IV, N V, O VI, Ne VIII, Mg X, Si XII, Fe XII) that should be sufficiently intense to be measurable at distances of $r = 3$ to $5R_\odot$ and perhaps further from Sun-center with a suitably designed coronagraphic instrument (Kohl *et al.*, 1981; Kohl and Withbroe, 1982). Also of interest are strong XUV ($150 < \lambda < 500$ Å) lines, particularly He II λ304 (see Ahmad, 1977) which provides information on alpha particles and lines from numerous ionization stages of iron, Fe IX to Fe XVI, which could be used to monitor the ionization states of iron in the solar wind near the Sun and probe the atmosphere using ions with different charges, but the same mass.

For most of these EUV and XUV lines the emergent intensity is a combination of collisionally excited and resonantly scattered components. The collisionally excited

© Kluwer Academic Publishers • Provided by the NASA Astrophysics Data System

1982SSRv...33...17W

component has an intensity (cf. Withbroe, 1970):

$$I_c(\lambda) = 0.86\,\lambda \int_{-\infty}^{\infty} A_{el} R_i N_e^2 C_{12} \phi_\lambda \, dx \,, \tag{10}$$

where $A_{el} = N_{el}/N_p$, N_{el} is the number of ions cm^{-3} summed over all stages of ionization of the atomic species producing the ion i, C_{12} is the collisional excitation rate coefficient, $R_i = N_i/N_{el}$ is the ionization balance term, N_i is the number of ions cm^{-3} of the ion species producing the line and ϕ_λ is the profile function (e.g. Gaussian for a Maxwellian particle velocity distribution function). The intensity of the resonantly scattered component is given by an equation identical to that for H I Lα (Equation (6)) except for the inclusion of the abundance A_{el} and use of R_i appropriate to the ion species involved. There may also be differences in the coefficients in the angular scattering function (see Equation (4)). For most ions collisional excitation dominates in the low corona, while at higher levels both radiative and collisional excitation are important (e.g. Figure 8a). The electron scattered component of these lines will be weak and blend into the 'continuum' produced by electron scattered disk radiation from the numerous weak lines in the EUV and XUV, the H I Lα continuum, He I continuum, etc.

The profile of the resonantly scattered component will be slightly narrower than that of the collisionally excited component due to the angular dependence of the scattering process (see Section 4), but the difference is very small and easily modeled (cf. Kohl and Withbroe, 1982). The relative contributions to the total intensity of the resonantly scattered and collisionally excited components can be evaluated using Equation (10) and the corresponding equation for the resonantly scattered component. Alternatively, for many lines one can use an empirical technique for separating the contributions of the two components as will be discussed in Section 7. The widths of EUV coronal lines are typically of the order of 0.05 to 0.1 Å for $T_i \approx 10^6$ K.

Spectral line profiles from ions can provide measurements of kinetic temperatures T_i of atomic species heavier than hydrogen. Measured in combination with the resonantly and electron scattered components of H I Lα, the spectral lines of heavier ions can provide critical data on mass-dependent or charge-to-mass dependent processes in the solar wind acceleration region.

7. Outflow Velocities

The intensity of a coronal resonance line depends on the number of particles in the line of sight capable of scattering radiation in the line and the intensity of the incoming radiation from the solar disk and lower levels of the corona. The number of scatterings is a function of the outflow velocity of the solar plasma. In a static atmosphere, the central wavelength of the coronal scattering profile is identical to that of the disk profile. However, in a region with solar wind flow the scattering profile is Doppler-shifted with respect to the disk profile, hence there is less efficient scattering resulting in a reduction in intensity of the scattered radiation. This effect is known as Doppler dimming (see

© Kluwer Academic Publishers • Provided by the NASA Astrophysics Data System

1982SSRv...33...17W

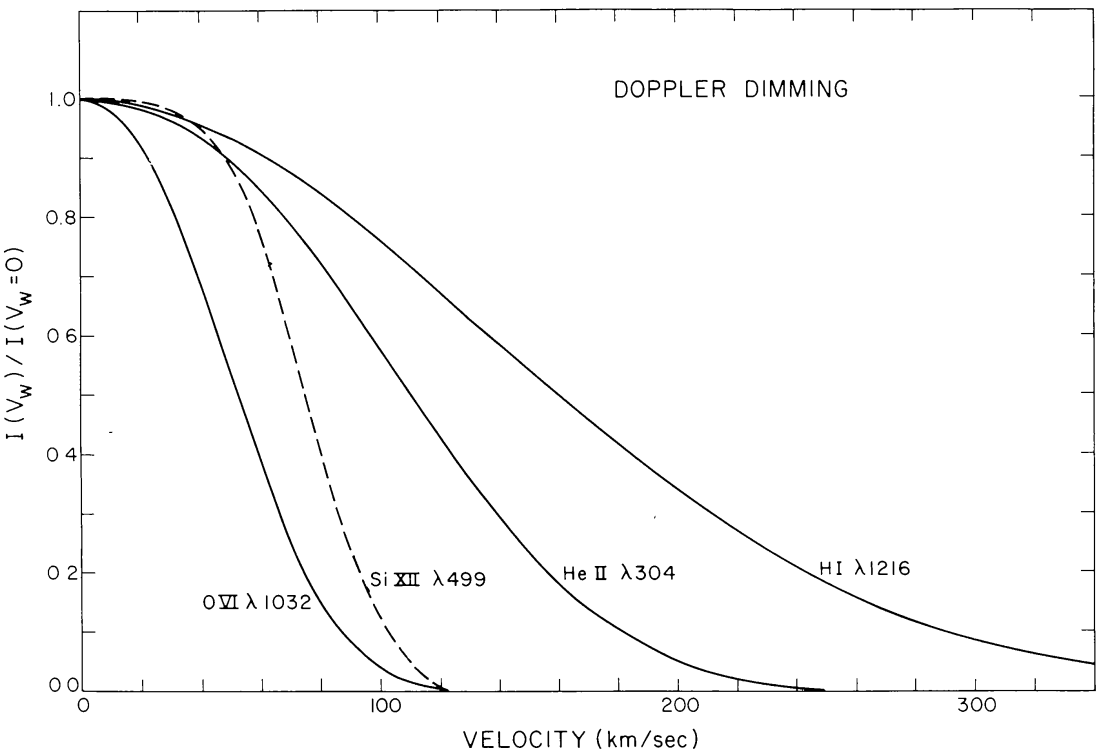

Fig. 7. Doppler dimming calculated for an isothermal corona with $T = 1.5 \times 10^6$ K (see text).

Hyder and Lites, 1970; Beckers and Chapman, 1973). Examples of the effect of Doppler dimming for several lines are illustrated in Figure 7. We see that the hydrogen Lα line is sensitive to flow velocities greater than about 100 km s^{-1}, while the other lines are sensitive to velocities above 30 to 60 km s^{-1} depending on the line.

How does one determine the amount of Doppler dimming? There are a variety of techniques for doing this (e.g. Kohl and Withbroe, 1982). These methods depend on comparing the intensity of a spectral feature that is affected by Doppler-dimming with the intensity of a spectral feature that is not. For example, a method suggested by G. Noci (personal communication) for hydrogen Lα makes use of the ratio of the intensity of the resonantly scattered component of a spectral line I_r and the intensity of the electron-scattered white light continuum. The intensity of the resonantly scattered component is given by (see Equation (6))

$$I_r = \text{const} \times \int_0^\infty A_{el} R_i N_e \bar{J} \, dx \tag{11}$$

where

$$\bar{J} = \int_{-\infty}^{\infty} J_\lambda \phi(\lambda - \lambda_w) \, d\lambda \,, \tag{12}$$

J_λ is the intensity of the disk radiation at wavelength λ, ϕ is the normalized absorption profile and λ_w is the Doppler shift introduced by the solar wind. (Equation (12) is an

© Kluwer Academic Publishers • Provided by the NASA Astrophysics Data System

1982SSRv...33...17W

approximation used here for illustrative purposes. A more precise formulation is given by Equation (6)). For an isothermal corona

$$I_r = \text{const} \times A_{el} \langle D_i(V_w) \rangle R_i \int_0^\infty N_e \, dx \,, \tag{13}$$

where $D_i(V_i)$ is the Doppler dimming term plotted in Figure 7. The intensity of the electron-scattered white light continuum is given by

$$I_{WL} = \text{const} \times \int_0^\infty N_e \, dx \,. \tag{14}$$

Hence, the ratio

$$\frac{I_r}{I_{WL}} \approx \text{const} \times A_{el} R_i \langle D_i(V_w) \rangle \,. \tag{15}$$

If the outflow velocities are sufficiently high to produce significant Doppler dimming, then the ratio I_r/I_{WL} will decrease with increasing flow velocity. Therefore, measurements of the ratio I_r/I_{WL} as a function of radius can be used to determine the amount of Doppler-dimming and, hence, the bulk outflow velocity of the observed ion. A first order estimate of the outflow velocity can be obtained by assuming (1) that the ionization balance term R_i is constant (which occurs if the corona is isothermal or the ionization balance is frozen in) and (2) that the elemental abundance A_{el} is constant (for hydrogen $A_{el} = 1$). In this case application of Equation (15) to measurements at several heights will provide relative outflow velocities. A more definitive analysis requires a self-consistent model of the observed region which makes use of temperatures, densities and geometry derived from the observations and calculated values of R_i. The requirement that the outward particle flux be conserved provides an additional constraint.

It is highly desirable to use redundant checks on outflow velocities. For example, in place I_{WL} one can use the intensity of the electron scattered component of Lα which also depends on $\int N_e \, ds$. This is particularly useful in the case of Doppler dimming determined from Lα observations, since the ratio of the intensities of the resonantly and electron scattered components of Lα is independent of the absolute calibration of the instrument used to make the measurements. Another check is provided by the ratio of the intensities of the resonantly scattered (I_r) and collisionally excited (I_c) components of spectral lines from ions. This ratio is sensitive to Doppler dimming. One can easily show that

$$\frac{I_r}{I_c} \approx \text{const} \times \langle D_i(V_w) \rangle \frac{\int_0^\infty N_e \, dx}{\int_0^\infty N_e^2 \, dx} \tag{16}$$

© Kluwer Academic Publishers • Provided by the NASA Astrophysics Data System

1982SSRv...33...17W

which is independent of A_{el} and R_i. The ratio I_r/I_c can be determined empirically for spectral lines in the lithium (e.g. N V, O VI, Ne VIII, Na IX, Mg X, Al XI, and Si XII) and sodium (e.g. Fe XVI) isoelectronic sequences, which account for the majority of the strong coronal resonance lines in the UV and EUV. The ions in these isoelectronic sequences produce a pair of resonance lines whose intensity ratio $I_{\lambda 1}/I_{\lambda 2}$ is a function of I_r/I_c (see Mariska, 1977; Kohl and Withbroe, 1982). (The resonantly scattered components of the two lines (e.g. Mg X $\lambda 610$, $\lambda 625$) have a 4 : 1 ratio, while the collisionally excited components have a 2 : 1 ratio.)

The Doppler-dimming techniques described above provide a means of obtaining information on outward flow velocities as a function of height above the solar limb. Doppler shifts of spectral lines provide information about flows directed toward or away from the observer. Flows that are symmetrical about the plane of the solar disk (e.g. spherically symmetric flows) can introduce line broadening in optically thin spectral lines measured above the limb, while unsymmetrical flows (e.g. plasma flowing outward in a bright streamer not in the plane of the disk) can produce Doppler shifts of spectral line profiles. The use of Doppler shifts for measuring flow velocities is particularly useful for observations of the low corona made using UV and EUV emission lines which can be observed on the disk. Such measurements can be used to map flow patterns in the transition region and lowest levels of the corona (cf. Cushman and Rense, 1976; Brueckner, 1980, Rottman *et al.*, 1981, 1982).

8. Charge States and Chemical Abundances

As discussed in Section 2, the ionization state of the solar wind is 'frozen in' within a few solar radii of the solar surface due to the rapid decline of density in the corona. Consequently, *in situ* measurements of charge states in the solar wind plasma at large distances from the Sun can provide information about the ionization balance in the solar wind acceleration region. However, due to the uncertainties in the physical conditions (temperatures, densities, flow velocities and geometry) in the acceleration region, the height at which 'freezing in' occurs cannot be determined reliably from these *in situ* solar wind measurements. An additional difficulty is that some charge states e.g. O VIII, may be affected significantly by nonthermal tails in the electron velocity distribution function (e.g. Owocki, 1982; Owocki and Scudder, 1982). Optical observations can provide critical data on physical conditions in the solar wind acceleration region that are needed for interpreting charge state measurements; the combination of the two types of measurements (spectroscopic and charge state) provide complementary data that can be used to probe the physics of this important region of the heliosphere.

Determinations of the chemical abundances in the solar wind plasma at 1 AU indicate that the abundances of elements heavier than hydrogen are extremely variable, by more than a factor of 4 (see review by Hirshberg, 1975). These large variations appear to be associated with dynamical phenomena in the solar corona and the types of coronal structures where the wind originates. Thus, measurements of abundances using spectroscopic information acquired from optical measurements of radiation from the

© Kluwer Academic Publishers • Provided by the NASA Astrophysics Data System

1982SSRv...33...17W

solar wind acceleration region are highly desirable in order to provide information on the magnitude and location of coronal abundance variations and thereby place constraints on the mechanisms producing these variations.

Measurements of the intensities of spectral lines can be used to obtain the desired information on chemical abundances and charge states. For example, for an isothermal corona Equation (6) yields for the ratio of the intensity of the resonantly scattered component of a spectral line at wavelength λ to that of hydrogen Lα:

$$\frac{I_r(\lambda)}{I_r(\lambda 1216)} = \text{const} \times \frac{A_{el} R_i D_i(V_w)}{R_{\mathrm{H\,I}} D_{\mathrm{H\,I}}(V'_w)} \,. \tag{17}$$

The Doppler-dimming terms can be evaluated as described above in Section 7. The electron temperature can be measured using the profile of the electron-scattered component of H I Lα, while the ionization balance term R_i can be calculated from empirically derived knowledge of T_e, N_e and the outflow velocity. Thus, one can obtain a determination of A_{el}. In some cases one may be able to measure several ions from the same parent element and thereby check the calculated ionization balance.

Clearly, it is highly desirable to acquire spectroscopic measurements in the solar wind plasma that later is sampled *in situ* by a spacecraft. For example, coronagraphic instruments in Earth orbit could observe radiation from the coronal plasma in a polar region whose plasma outflow is being studied by the International Solar Polar Mission spacecraft.

9. Observational Considerations

Figure 8a gives predicted intensities as a function of radius for H I Lα and Mg X λ610. These intensities were calculated using Saito's (1970) density model. For simplicity, the atmosphere was assumed to be isothermal with a temperature $T = T_e = T_p = T_i = 2 \times 10^6$ K. Intensities were calculated for a static model and one with solar wind outflow where the particle flux nVr^2 = constant with the constant corresponding to a proton flux at 1 AU equal to 3.8×10^8 cm^{-2} s^{-1} (cf. Feldman *et al.*, 1977). Intensities in streamers could be a factor of 5 to 50 times higher than those derived from Saito's model because of the higher densities in these features. In coronal holes the intensities could be a factor of 2 or more lower depending upon the spectral line, density in the hole and the outflow velocities (e.g. Kohl and Withbroe, 1982). We will discuss Lα further in Section 10 when we consider applications to existing observations.

With a UV/EUV coronagraph such as the one defined for Spacelab (Kohl *et al.*, 1981) an integrated intensity of 5×10^6 photons cm^{-2} s^{-1} str^{-1} yields a count rate of a 1 Hz or more (for a spatial resolution of $0.15' \times 4'$ and spectral resolution 0.1 Å) which is adequate for observing many spectral lines out to 3 to $5R_\odot$ and even further for the strongest lines, particularly Lα (Kohl and Withbroe, 1982). For measurements of the electron scattered H I Lα an integrated intensity of 10^6 photons cm^{-2} s^{-1} sterad^{-1} yields a count rate of 1 Hz (for $4' \times 4'$ spatial resolution, 10 Å spectral resolution). This is adequate for line profile measurements out to $4R_\odot$ in equatorial regions.

© Kluwer Academic Publishers • Provided by the NASA Astrophysics Data System

1982SSRv...33...17W

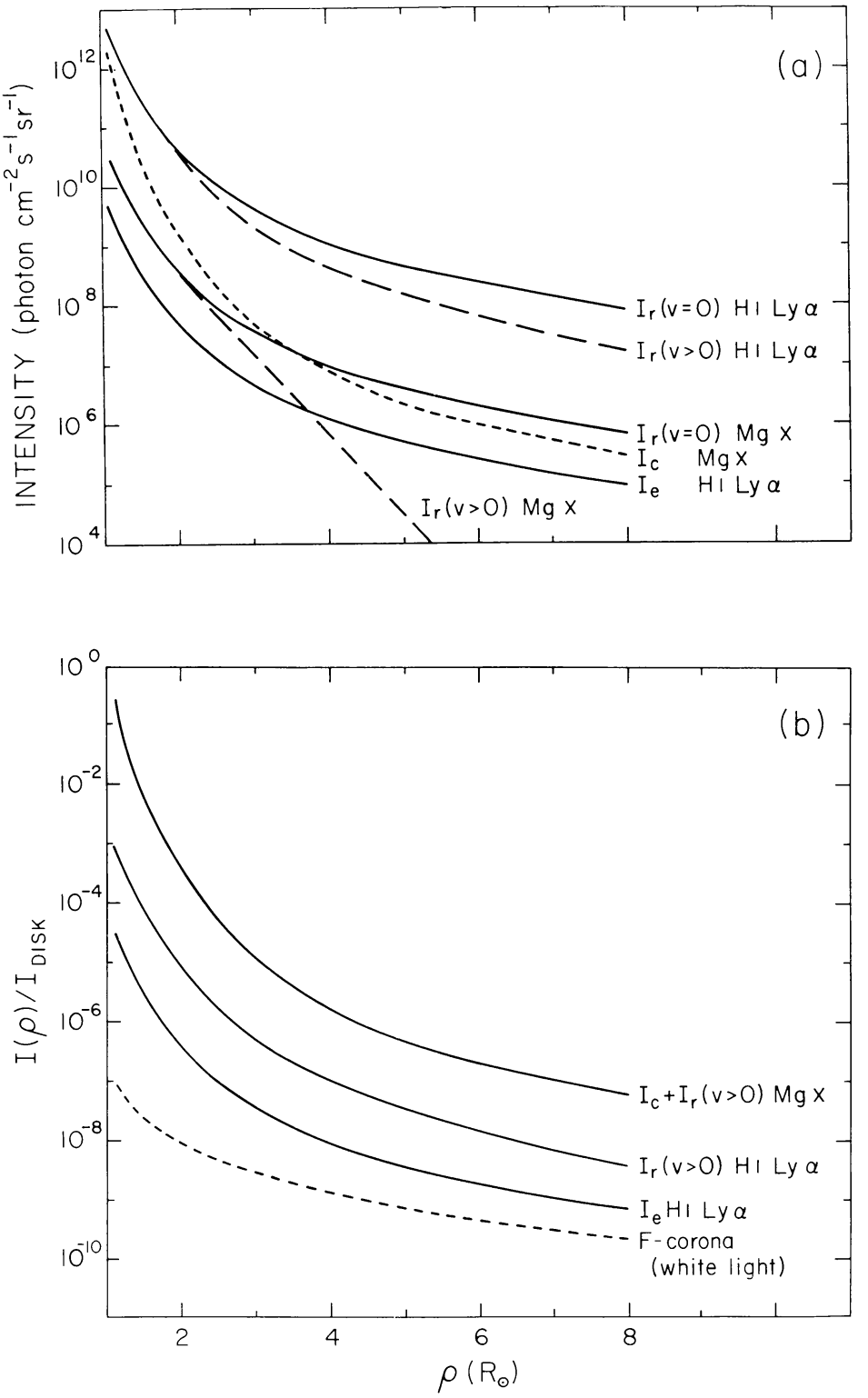

Fig. 8. (a) Intensity as a function of distance ρ from Sun center calculated using a model for typical equatorial region. Curves are given for the resonantly scattered I_r and electron scattered I_e components of H I Lα and the resonantly scattered and collisionally excited I_c components of Mg λ610. Intensities $I_r(V = 0)$ were calculated for a static model and $I_r(V > 0)$ were calculated for a model with solar wind flow (see text). (b) Intensity in units of the disk intensity as a function of ρ for a model of typical equatorial region with solar wind flow. The curve for electron scattered H I Lα is described in the text. For comparison the intensity of the white light *F*-corona is also given. In the UV and EUV the *F*-corona may be less intense (in units of the disk brightness) by a factor of 2 to 3 (see text).

© Kluwer Academic Publishers • Provided by the NASA Astrophysics Data System

1982SSRv...33...17W

It should be emphasized that coronagraphic instruments are needed for observations beyond $\rho \gtrsim 1.4 R_\odot$ because of the requirement to reject stray light from the disk. Normal incidence optical telescopes without occulting systems flown on spacecraft such as the Orbiting Solar Observatories (OSO) and Skylab have had stray light rejections of the order of 10^{-3} (e.g. Harvard Skylab, OSO-4 and OSO-6 EUV instruments). Although this level of stray light rejection is perfectly adequate for measurements made on the disk and near the solar limb ($\rho \lesssim 1.4 R_\odot$) in EUV coronal lines like Mg X λ610, it is inadequate for measurements made at greater distances from the limb. For Lα a stray light rejection of 10^{-3} is inadequate at all heights above the limb. This is illustrated by the information presented in Figure 8b which gives values of the ratio $I(\rho)/I_{\text{disk}}$ where $I(\rho)$ is the coronal intensity from Figure 8a and I_{disk} is the intensity of the radiation from the solar disk.

For a signal (from coronal radiation) to noise (from stray light) ratio $\gtrsim 10$, the on-band stray light rejection required for the resonantly scattered Lα line should be approximately 10^{-7} to 10^{-8} for observations out to $\rho \approx 4 R_\odot$ depending on the type of feature being observed. For measurements beyond $\rho \approx 6 R_\odot$ a stray light rejection of an order of magnitude better is desirable. For the Mg X line, whose behavior is representative of EUV spectral lines from heavier ions, the requirements for stray light rejection are approximately a factor of 10 less stringent than for the resonantly scattered component of Lα. This comes from the smaller difference between the disk intensity for λ610 and its intensity beyond the limb.

To specify the on-band stray light requirement for measurements of the electron scattered profile, we must first identify the wavelength bands to be observed. The central 4 to 5 Å of the electron scattered profile is masked by the resonantly scattered component and also would have an unacceptable stray light level due to the intensity of the chromospheric Lα emission. There are also several strong spectral lines (e.g. C III λ1175, N I λ1200, Si III λ1206, H I λ1216, N V λ1238, N V/Fe XII λ1243, and Si III λ1264) which can be spectrally isolated. The remaining disk radiation in the wavelength range of interest consists of continuum plus weak spectral lines that can be treated as continuum for this purpose. Measurements of EUV disk spectra (Dupree and Reeves, 1971; Dupree *et al.*, 1973; Vernazza and Reeves, 1978) suggest that this quasi-continuum has a relatively constant value of about 2.5×10^{12} photons cm^{-2} s^{-1} sterad^{-1} Å^{-1}. Taking this value for I_{disk} we obtain for $I_e(\rho)/I_{\text{disk}}$ the curve given in Figure 8b, where I_e is the intensity of the electron scattered component of H I Lα at line center for $T_e \approx 2 \times 10^6$ K. An acceptable stray light for this line would be about 10% of the line center intensity which implies a requirement for stray light rejection approximately an order of magnitude more stringent than those for the resonantly scattered component (but an order of magnitude less stringent than for white light observations of the *K*-corona). If the instrumental stray light contribution is known so that it can be subtracted from the observations, then a higher level of stray light can be tolerated. One possible technique for doing this is through measurements of the intensity at the wavelengths of strong lines such as Si III λ1206 and C II λ1335 whose scattered coronal radiation is expected to be much lower than that of EUV coronal lines and H I Lα due to the small abundance at coronal temperatures of the scattering ions. One can also make

© Kluwer Academic Publishers • Provided by the NASA Astrophysics Data System

1982SSRv...33...17W

broad-band measurements at wavelengths outside the spectral region where the coronal lines contribute significantly to the intensity.

A capability for suppression of off-band photospheric radiation from the visible and near UV is also required. This is extremely critical because of the large intensity of the photospheric radiation at these wavelengths. For observations at $\rho \lesssim 3.5 R_\odot$ the necessary suppression of on-band and off-band radiation has been demonstrated by a rocket UV coronagraph which uses an externally and internally occulted telescope together with a scanning spectrometer and solar blind photoelectric detector (Kohl *et al.*, 1978, 1980).

Interpretation of measurements of Lα coronal radiation must also take into account the effects of geocoronal absorption (scattering) and emission ($I \approx 10^9$ photon $cm^{-2}\,s^{-1}\,sterad^{-1}$ near solar maximum). Neutral hydrogen in the geocorona scatters photons out of the central portion of the coronal Lα profile, while Lα emission from the geocorona contributes photons near line center. Close to the Sun, where the coronal

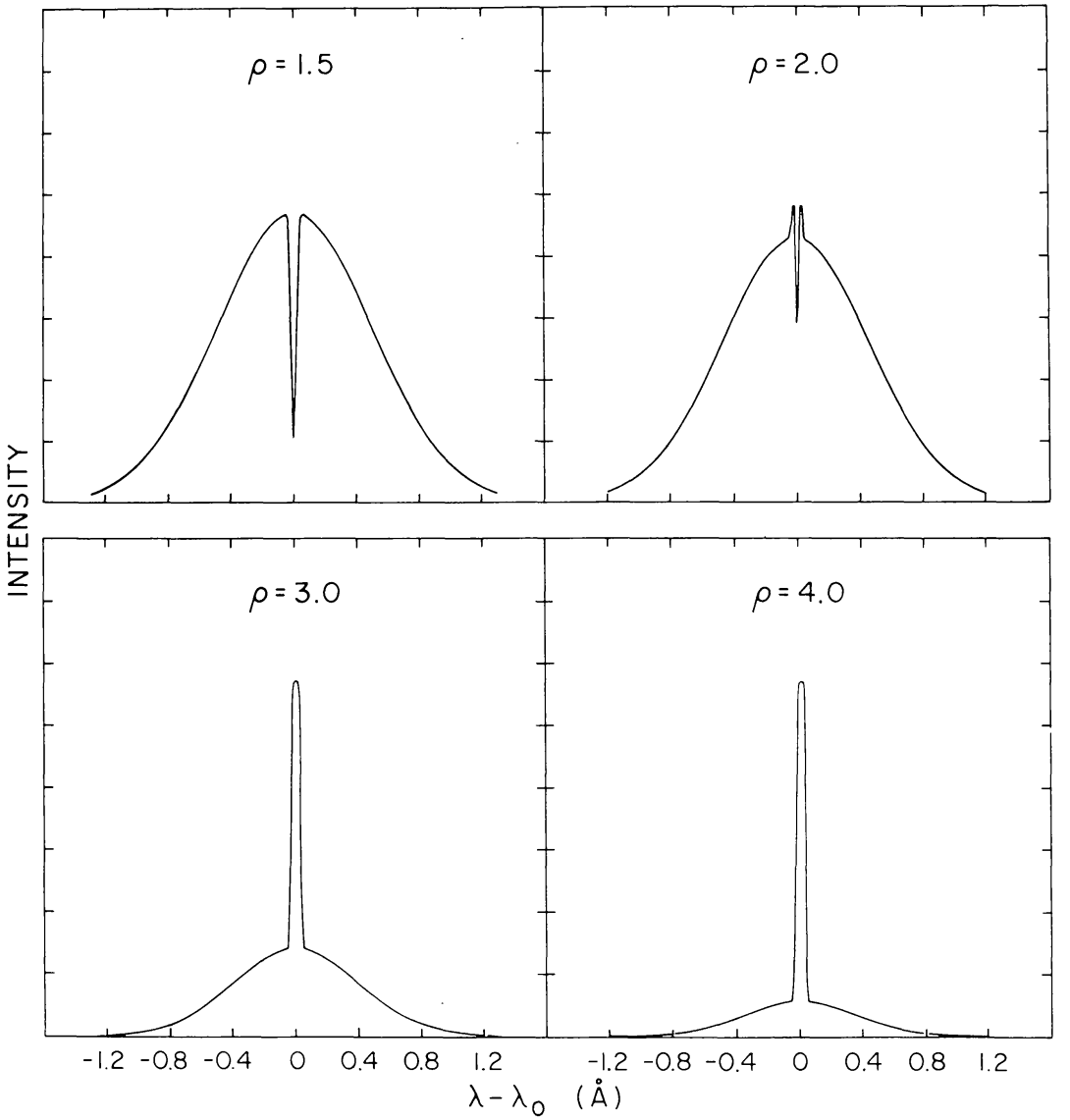

Fig. 9. Calculated geocoronal absorption/emission contribution to profiles of H I Lα from a typical equatorial region.

© Kluwer Academic Publishers • Provided by the NASA Astrophysics Data System

1982SSRv...33...17W

intensities are large, the effects of the geocoronal absorption are more important than those due to the geocoronal emission; at distances beyond about $2R_\odot$ the effects of the geocoronal emission are more important. This is illustrated in Figure 9 for a set of profiles with intensities typical of equatorial regions. Because the geocoronal absorption/emission feature is much is much narrower than the profile of the solar line, the effects of the geocorona can be accounted for through use of measurements made with sufficiently high spectral resolution (≈ 0.1 Å), a value readily attainable. There is another narrow emission component of much lower intensity ($I \approx 4 \times 10^7$ photon $cm^{-2}\ s^{-1}$ sterad^{-1}), the interplanetary Lα emission component whose contribution is negligible for measurements made at $\rho < 3.5R_\odot$. At greater distances where its contribution may be non-negligible, its effects can be eliminated through use of measurements made with good spectral resolution (≈ 0.1 Å).

Scattering by dust in the solar corona and interplanetary space also contributes to the coronal emission spectrum. At the present time there is very little empirical information on the brightness of the dust scattered or *F*-component in the UV and EUV. Shortward of $\lambda 1500$ the only measurement (Kohl *et al.*, 1980) is an *upper limit* at $\lambda 1216$ which is 10^{-7} of the disk intensity at $\rho = 3.5R_\odot$ in a polar region. Theoretical calculations of the spectrum of the *F*-corona using Mie theory suggest that its brightness (in units of the disk brightness at λ) varies as $\lambda^{1/2}$ (e.g. Van de Hulst, 1957; Roser and Staude, 1978). Measurements of the *F*-corona at wavelengths from $\lambda 2000$ to $\lambda 8000$ are consistent with this prediction (e.g. Blackwell *et al.*, 1967; Orrall and Speer, 1973; Roser and Staude, 1978). Whether or not the $\lambda^{1/2}$ behavior continues to shorter wavelengths is not known. Lillie (1972) found that the brightness of the zodiacal light measured at elongations greater than 50° from the Sun increased rapidly with decreasing wavelength between 2000 and 1600 Å. Orrall and Speer (1973) suggested the possibility that the brightness of the *F*-corona could exhibit a similar increase and were not able to rule this possibility out on the basis of UV measurements made during the 1970 solar eclipse. However, more recent experimental and theoretical work on the brightness of the zodiacal light indicates that Lillie's (1972) measurements are probably too high (cf. Roser and Staude, 1978; Weinberg and Sparrow, 1978; Henry *et al.*, 1980). Furthermore, the brightness of the zodiacal light at elongations greater than about 50° is dominated by reflection from the dust, while the intensity of the *F*-corona is dominated by diffraction which is expected to give a reddened spectrum (cf. Ingham, 1961; Roser and Staude, 1978). Until better information is available it appears reasonable to assume that the theoretical calculations of the spectrum of the *F*-corona are valid and therefore that the brightness of the *F*-corona varies as $\lambda^{1/2}$.

The dotted line in Figure 8b gives the measured intensity of the *F*-corona in white light (in units of the disk intensity). If the intensity of the *F*-corona in the UV and EUV is equal to or less than these values as implied by the theoretical calculations discussed above, then the contribution of the *F*-corona can be ignored in the interpretation of measurements of the resonantly scattered and collisionally excited components of UV and EUV spectral lines for $\rho \lesssim 8R_\odot$.

There are two components of the *F*-coronal radiation that need to be considered in

© Kluwer Academic Publishers • Provided by the NASA Astrophysics Data System

1982SSRv...33...17W

the interpretation of observations of the electron scattered Lα radiation. The first of these is the dust scattered Lα disk radiation. This component, which has a FWHM ≈ 0.5 Å, can be easily separated from the electron scattered radiation due to the two order of magnitude difference in the line widths. (The same argument applies to separation of the resonantly scattered radiation, which as indicated above, is expected to have an intensity much larger than that of the *F*-corona.) The on-band contribution from the *F*-corona poses more of a problem. This radiation is due to the dust scattering of the UV 'continuum' near Lα. If the intensity of the *F*-corona at wavelength λ (in units of the disk intensity at λ) varies as $\lambda^{1/2}$, then at wavelengths near $\lambda 1216$ this component will have an intensity approximately a factor of 2 smaller than the values given by the dotted curve in Figure 8b. If this is the case, then the contribution of the *F*-corona can be ignored in the interpretation of observations of the electron scattered in the low corona at heights corresponding to $\rho < 2R_\odot$. For observations made at greater distances the contribution of the *F*-corona should be taken into account. In equatorial regions the intensity of the *F*-corona is expected to be a factor of 5 to 10 smaller than the total intensity of the electron scattered component of Lα at $\rho = 2.5R_\odot$ and not reach equal intensity until $\rho \gtrsim 8R_\odot$. This is marked contrast to the situation in the visible where the intensity of the white light *F*-corona equals that of the electron scattered or *K*-corona in equatorial regions for $\rho \approx 2.5R_\odot$ and is several times larger by $\rho \approx 5R_\odot$.

Because of the lack of experimental verification that the brightness of the *F*-corona in the UV is as predicted by theory, improved measurements are needed. This is particularly important for achieving reliable measurements of electron scattered Lα radiation from the corona. This can be accomplished by making measurements at strong lines such as Si III $\lambda 1206$ as suggested earlier for measuring instrumental stray light. The latter contribution can be determined in the laboratory. Whether the undesired scattered disk radiation is due to stray light in the instrument or dust near the Sun is not significant for the purpose of measuring T_e, what is important is a capability of separating the signal from the dust and instrumental stray light from the signal due to scattering from coronal electrons. An alternative possiblity for separating the contributions of the electron scattered and *F*-components is to make use of the polarization of the electron scattered radiation as is commonly done in the visible.

10. Results of Initial Observations

At the present time there exists only a very limited amount of UV and EUV spectroscopic data from the solar corona beyond $r = 1.5R_\odot$. These data were acquired with a UV coronagraph employing reflecting optics (cf. Kohl *et al.*, 1978). This instrument and a companion white light coronagraph were carried above the UV absorbing layers of the terrestrial atmosphere by a sounding rocket. There have been two flights, both near the time of solar maximum, one in 1979 and the other in 1980 (Kohl *et al.*, 1980; Wieser *et al.*, 1981).

The primary objective of the 1980 flight was to study a coronal hole located at the southern solar pole. Coronal holes are thought to be a major source of solar wind,

© Kluwer Academic Publishers • Provided by the NASA Astrophysics Data System

1982SSRv...33...17W

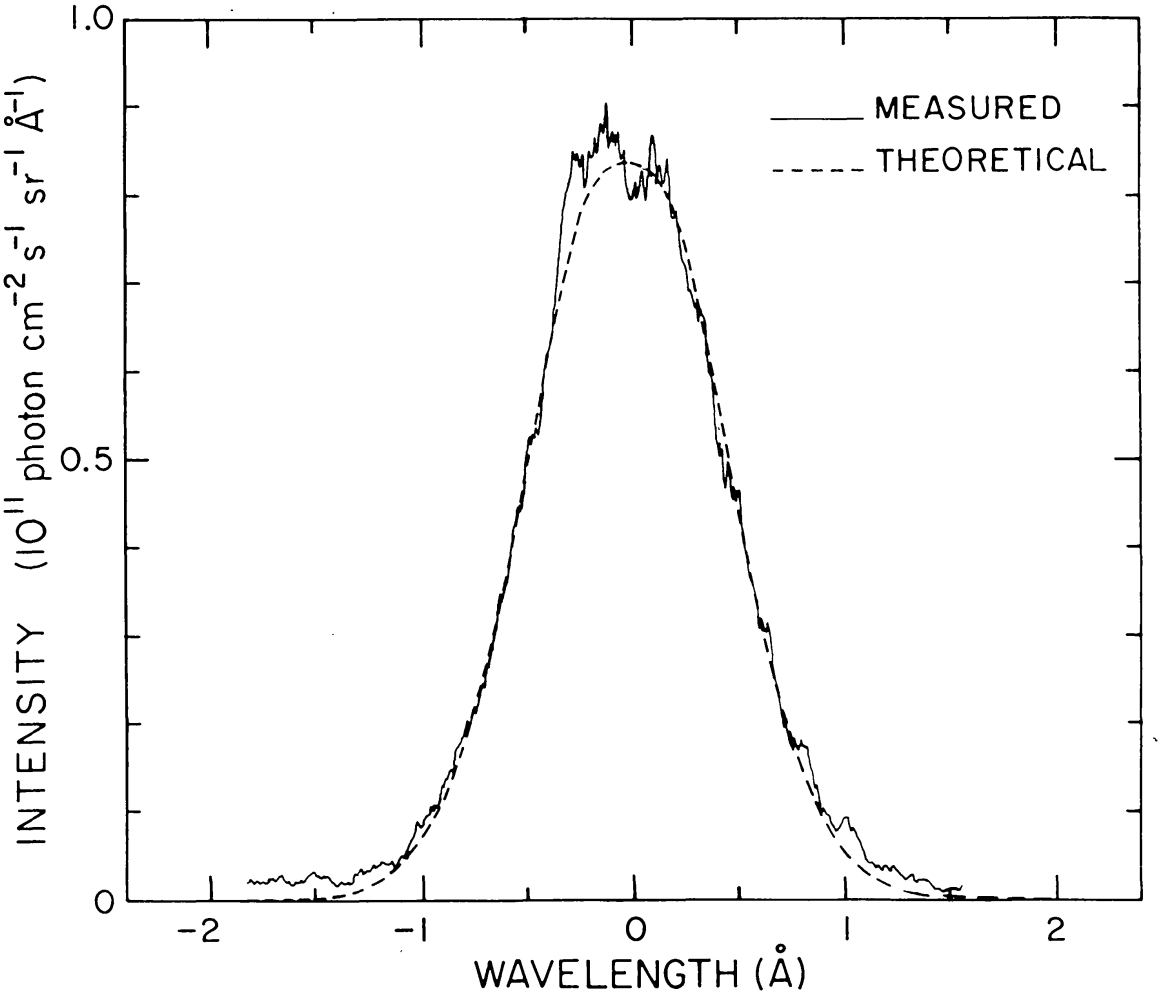

Fig. 10. A comparison of an empirical (solid line) and theoretical (dashed line) profiles of the resonantly scattered component of Lα. The empirical profile was measured in a polar region near the edge of a coronal hole. The theoretical profile has been convolved with the instrumental profile which has a FWHM = 0.35 Å.

particularly high speed solar wind streams. Consequently, coronagraphic determinations of plasma parameters of these features are of considerable importance. An example of the quality of the spectroscopic data that can be obtained with a UV coronagraphic instrument is shown in Figure 10 which presents an empirical profile (solid line) of the resonantly scattered component of hydrogen Lα measured at $\rho = 1.8 R_{\odot}$ in the polar region observed in the 1980 rocket flight. The parameter ρ is the distance measured in solar radii from Sun-center to the point where the line of sight intersects the plane of the disk. The empirical profile has been fit with a profile calculated for an isothermal corona. This illustrates how well this particular observation is represented by a Maxwellian velocity distribution function for the hydrogen atoms along the line of sight. The theoretical profile has lower intensities in the line wings; however, until a more detailed analysis of the data is completed, we will not know whether or not this is significant.

As discussed in Sections 3 and 4 measurements of spectral line profiles provide information on kinetic temperatures in the region where the spectral line radiation

© Kluwer Academic Publishers • Provided by the NASA Astrophysics Data System

1982SSRv...33...17W

originated. By measuring profiles at several heights in the corona one can obtain information on the temperature gradient in the observed region. Figure 11 shows hydrogen kinetic temperatures determined from Lα profiles measured at several positions ρ on a radius vector directed along the axis of the coronal hole that was centered on the south solar pole during February 1980. The profiles measured at ρ = 1.5, 2.5, and 3.0 $R_\odot$ had nearly identical widths implying that the hydrogen kinetic temperature was nearly constant ($T_{\mathrm{H\,I}} \approx 10^6$) over the height range where the line profiles were formed r = 1.5–4 $R_\odot$. Measured temperatures are plotted at the radii (r = 1.7, 3.1, and 3.8 $R_\odot$) corresponding to the mean heights where the radiation observed at ρ = 1.5, 2.5, and 3.0 $R_\odot$ originated (see Withbroe *et al.*, 1982). The magnitude of the error estimates given depend upon the uncertainties in fitting the profiles with a Gaussian curve and the uncertainties in the correction for the effects of geocoronal emission/absorption near line center (cf. Withbroe *et al.*, 1982). The solid line is the inferred run of temperature. It should be emphasized that this is a kinetic temperature and includes the effects of both thermal and non-thermal motions broadening the Lα line profiles.

For comparison we have plotted temperatures predicted by a simple two-fluid model with no plasma heating above the base of the corona (cf. Hartle and Sturrock, 1968;

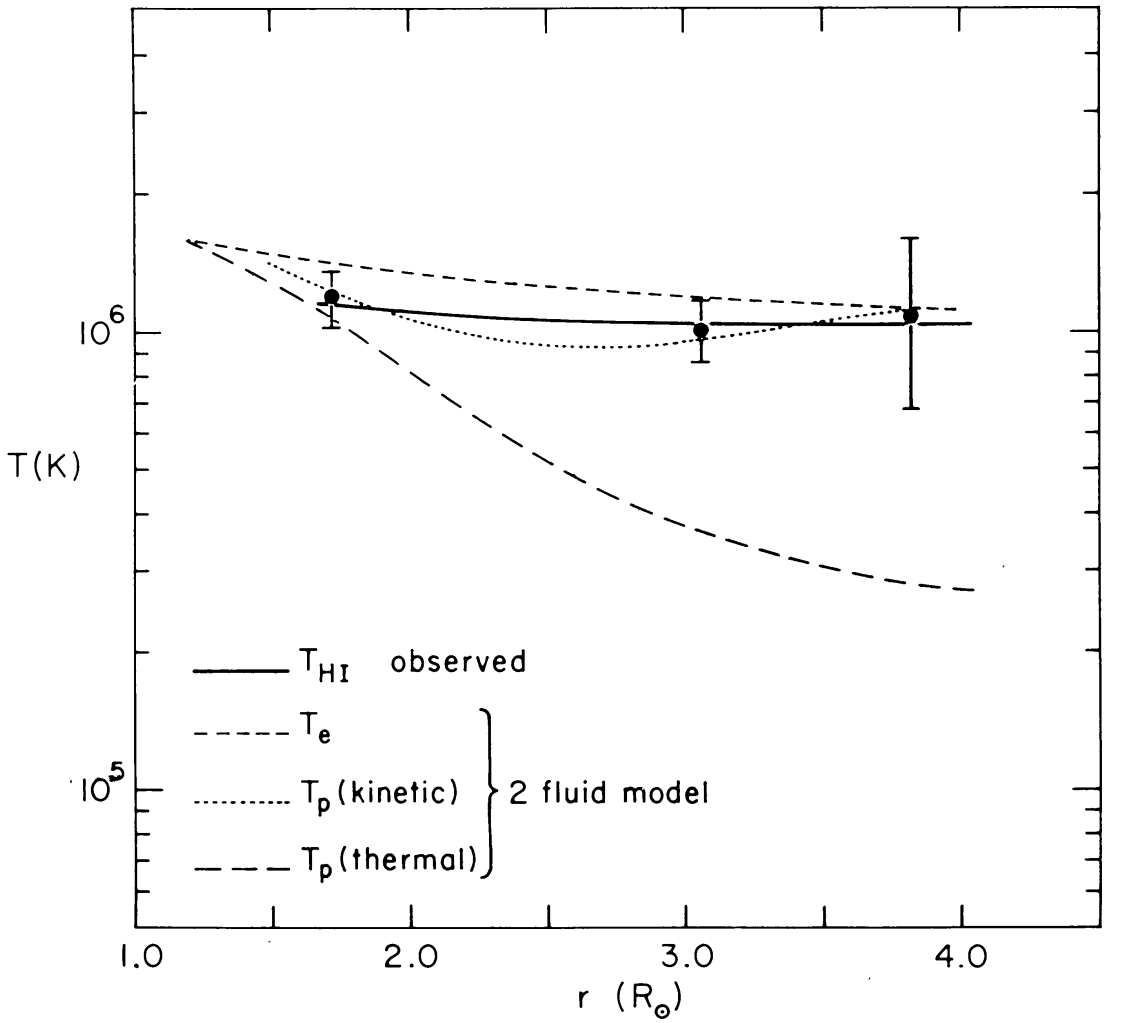

Fig. 11. A comparison of empirical and theoretical temperatures in a polar coronal hole (see text).

© Kluwer Academic Publishers • Provided by the NASA Astrophysics Data System

1982SSRv...33...17W

Nerney and Barnes, 1977; Hollweg, 1978). The short dash line gives the run of electron temperature with radius, while the long dash line gives the predicted proton thermal temperatures. The electron and proton temperatures diverge with height due to the rapid decrease in electron-proton coupling with decreasing density. The electron temperature has a shallow temperature gradient due to the high thermal conductivity of electrons, while the proton temperature falls off nearly aiabatically. We obtained an estimate of the electron temperature from the ratio of the Lα and white light intensities. This ratio depends on the ionization balance of hydrogen which is primarily a function of the electron temperature (see Gabriel, 1971). The value obtained, 1.5×10^6 K for $r = 1.7 R_\odot$, provides a boundary condition for the assumed two fluid model.

Because of the strong coupling between coronal hydrogen atoms and protons in the observed height range, one expects the hydrogen and proton kinetic temperatures to be equal. The difference between the observed coronal hydrogen kinetic temperatures and the calculated proton thermal temperatures indicates that the assumed model is inadequate. One way of bringing the calculated and observed temperatures into agreement is to increase the rms velocity of the protons. There are several ways of accomplishing this. One way is through extended proton heating in the region 1.5 to $4 R_\odot$. Addition of thermal energy by a mechanism with an energy dissipation length of about $4 R_\odot$ could explain the observations. A similar result was obtained from measurements in an unstructured 'quiet' region of the solar corona observed during the 1979 flight of the rocket coronagraphs. See Withbroe *et al.* (1982) for details.

Energy carried by waves could also be contributing to the rms motions of the protons. Consider Alfvén waves which have been suggested as a possible source of energy and momentum for plasma heating and/or solar wind acceleration in coronal holes (see review by Hollweg, 1981). For non-dissipating Alfvén waves Hollweg gives $N^{1/2} \langle v^2 \rangle$ = constant where v is the rms velocity amplitude of the waves and $N = N_e = N_p$. If the rms velocity is specified at one height, then this relationship can be used to calculate the rms velocity at other heights from the measured variation of density N with height. The dotted line gives the predicted proton kinetic temperature obtained by assuming

$$T_p(\text{kinetic}) = T_p(\text{thermal}) + T_A$$

with

$$T_A = m \langle v^2 \rangle / 2k = m \times \text{constant}/2kN^{1/2},$$

where the constant was adjusted to give the best fit to the observations. The adopted value of the constant corresponds to $v_{\text{rms}} = 115 \text{ km s}^{-1}$ at $r = 4R_\odot$. This is about two-thirds the value suggested by Hollweg (1981) for this height.

The fit between the calculated and observed kinetic temperatures is sufficiently good to suggest that plasma motions due to Alfvén waves may be contributing significantly to the broadening of the H I Lα. The shapes of the line profiles, which are nearly Gaussian, place a constraint on the spectrum of these Alfvén waves, if they are present. It is important to note that there are other explanations for the nearly constant width

© Kluwer Academic Publishers • Provided by the NASA Astrophysics Data System

1982SSRv...33...17W

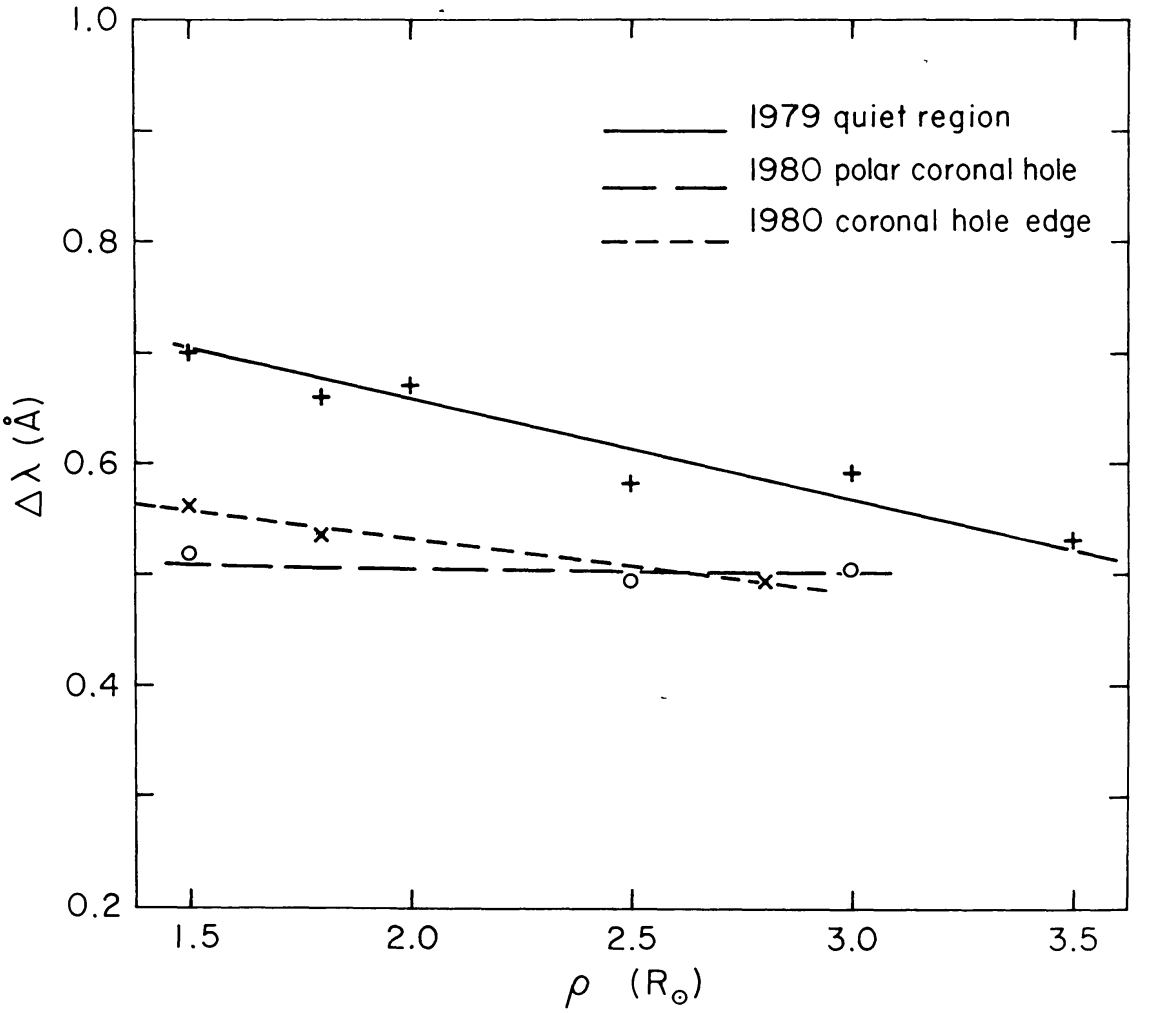

Fig. 12. Widths ($1/e$ half width $\approx 0.6 \times$ FWHM) of resonantly scattered H I Lα measured in 3 coronal regions.

of the Lα line, such as the above mentioned extended proton heating. In order to distinguish between thermal and non-thermal line broadening mechanisms, additional empirical constraints are needed, such as measurements of spectral lines from ions with different masses.

In order to illustrate the differences that can occur between different regions of the corona we have plotted in Figure 12 hydrogen Lα widths ($1/e$ half width $\approx 0.6 \times$ FWHM) for the three best observed regions in the 1979 and 1980 flights of the Rocket Lyman Alpha Coronagraph. For these three sets of data the spectral line widths are either constant or decreasing with increasing radius for $1.5 \leq \rho \leq 3.5 R_\odot$. This indicates that the hydrogen kinetic temperatures were nearly constant or decreasing with increasing radius in the observed regions. Because of the sensitivity of the hydrogen kinetic temperature to energy deposition mechanisms that heat protons, this places tight upper limits on the amount of direct proton heating between $r = 1.5$ and $4 R_\odot$ (cf. Withbroe *et al.*, 1982). The differences in the magnitude of the line widths indicates that significant differences in proton kinetic temperatures between different regions are possible. For example, the kinetic temperature at $r = 1.7 R_\odot$ (the mean height of

© Kluwer Academic Publishers • Provided by the NASA Astrophysics Data System

1982SSRv...33...17W

formation of the Lα radiation observed at $\rho = 1.5 R_\odot$) is approximately 2.2×10^6 K in the quiet region observed in 1979 and 1.1×10^6 K in the polar coronal hole observed in 1980. Another polar coronal hole observed during the 1979 flight had an intermediate kinetic temperature, 1.8×10^6 K (Kohl *et al.*, 1980) at similar heights.

These few measurements suggest that coronal temperatures in the solar wind acceleration region vary from structure to structure reflecting differing amounts of coronal energy input. This is not surprising given the variation in plasma heating found at lower levels of the corona (see review by Withbroe and Noyes, 1977). More extensive observations, such as can be obtained by satellite experiments, are required before one can seek possible relationships between coronal structure (open or closed magnetic structures, streamers, coronal holes etc.) and the spatial variations of coronal temperatures determined from a given particle species such as hydrogen atoms.

As indicated in Section 7, the ratio of the intensities of the hydrogen Lα line and the white light continuum provides an empirical constraint on solar wind outflow velocities. For the 1980 observations the measured ratio of the intensities of the Lα line and white light continuum was nearly independent of height. This indicates that the flow velocity of the plasma emitting the observed Lα and white light radiations was less than about 100 km s^{-1}, that is, the velocities were sufficiently low that the Lα line was not significantly affected by Doppler-dimming (see Figure 7). In order to define the limits on the outflow velocities more carefully, the measured Lα intensities where compared

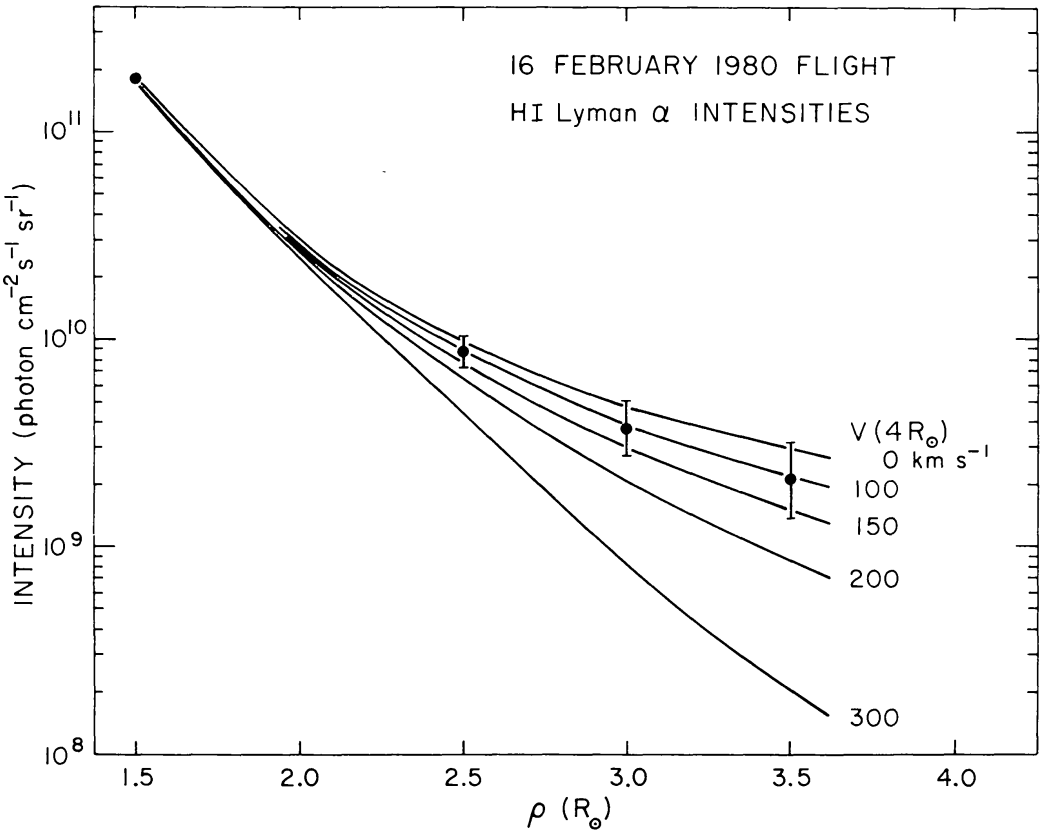

Fig. 13. A comparison of measured (points) and calculated (curves) H I Lα intensities as a function of distance from Sun center. The curves give values calculated for models with different solar wind fluxes parameterized here by the wind velocity at $4R_\odot$ (see text).

© Kluwer Academic Publishers • Provided by the NASA Astrophysics Data System

1982SSRv...33...17W

with those calculated from a series of coronal models (see Figure 13). The intensity of the scattered Lα radiation depends on the shape of the coronal scattering profile, the number of neutral hydrogen atoms in the line of sight (which can be calculated from the electron density and the electron temperature which determines $N_{\mathrm{H\,I}}/N_e$) and the solar wind velocity. The width of the Lα scattering profile was measured and the electron densities were determined from measurements of the polarization and brightness of the white light corona. The electron temperature at $r = 1.7\,R_\odot$ was determined from the observations as discussed above and for other heights was assumed to vary as $r^{-2/7}$ (e.g. the same as in Figure 11). Use of a model with an isothermal electron temperature yields similar results due to the insensitivity of the Lα intensity to variations in the electron temperature (e.g. Withbroe *et al.*, 1982). For the radial variation of the solar wind velocity V was assumed a constant outward particle flux NVr^2.

The upper curve in Figure 13 is for a static atmosphere. The other curves show the predicted Lα intensities for models with different outward particle fluxes parameterized by the velocity at $r = 4\,R_\odot$. At low heights where the density is high and solar wind velocity is low there is little Doppler dimming. However, due to the steady increase in flow velocity with increasing height, the amount of Doppler dimming increases with height causing the intensity to diverge from that calculated for the static model. A comparison of the calculated intensities with those measured confirms that the amount of Doppler dimming over the observed range of heights is small, corresponding to flow velocities at $r = 4\,R_\odot$ of less than about 150 km s^{-1}. Given that the sound speed for a corona with T_e = 1 to 1.5 × 10^6 K is 130 to 160 km s^{-1}, the observations suggest that the solar wind flow in the observed plasma was subsonic for $r \lesssim 4\,R_\odot$ and thus that the critical point was at $r \gtrsim 4\,R_\odot$. Lα measurements in an unstructured 'quiet' region of the corona observed in April 1979 also showed little or no Doppler-dimming consistent with subsonic flows for $r \leq 4\,R_\odot$ (Withbroe *et al.*, 1982). A more detailed inhomogeneous model for the polar region observed in 1980 is being developed from ground-based synoptic coronal data, 1980 eclipse measurements and data from the rocket coronagraphs (Munro *et al.*, 1982). This model should yield tighter constraints on the range of possible flow velocities in this region.

Analyses of observations acquired in the 1979 and 1980 flights of the CfA/HAO rocket coronagraphs yields the following empirical constraints on theoretical models for the solar wind acceleration region:

- nearly Gaussian H I Lα profiles;
- nearly constant or decreasing hydrogen kinetic temperatures or $1.5 < r < 4\,R_\odot$;
- subsonic flow for $r < 4\,R_\odot$ (critical point at $r \gtrsim 4\,R_\odot$);
- an upper limit of 140 km s^{-1} for the rms velocity of waves capable of broadening the Lα line for $r \approx 4.0\,R_\odot$;
- some evidence for extended proton heating or a non-thermal contribution to the motions of H I atoms in the observed regions.

For a more detailed discussion of results of the 1979 and 1980 flights of the rocket coronagraphs see Kohl *et al.* (1980, 1982), Munro *et al.* (1982); and Withbroe *et al.* (1982).

© Kluwer Academic Publishers • Provided by the NASA Astrophysics Data System

1982SSRv...33...17W

11. Future Observational Programs

In the above sections we have discussed some of the possibilities for probing the physical conditions in the solar wind acceleration region through use of UV and EUV spectroscopy. We have also briefly summarized results of preliminary steps in implementing UV spectroscopy of this critical region of the solar atmosphere made possible by brief rocket flights of coronagraphic instruments on sounding rockets. Future sounding rocket or Detached Shuttle Payload flights are expected to provide additional information about the physical conditions in the solar wind acceleration region and thereby provide additional empirical constraints on solar/stellar wind theory. For example, the existing Rocket Lyman Alpha Coronagraph is being modified to measure the integrated intensities of the O VI resonance lines at $\lambda 1032$ and $\lambda 1037$. These lines are much more sensitive to low speed flows ($30 < V < 100$ km s^{-1}) than the Lα line (see Figure 7). Measurements with the O VI line will provide tighter constraints on the magnitude of the solar wind flow velocities within a few solar radii where subsonic flows have been indicated in the first two flights of the Lyman Alpha Coronagraph. A subsequent modification under study is the addition of an array detector that will permit measurement of the electron scattered component of the hydrogen Lα line.

Sounding rocket and Detached Shuttle Payload flights are extremely useful for proof testing the spectroscopic diagnostic techniques. However, to achieve the full capabilities of UV/EUV coronagraphic instruments, experiments in long term orbital flights are required to provide the observing time needed (1) to measure the weak coronal emission over a wide range of heights in a variety of coronal structures, (2) to obtain synoptic observations for probing the three dimensional structure of the corona and its temporal variations, and (3) observing coronal transient phenomena. The availability of long observing times is particularly important for measuring profiles of spectral lines other than resonantly scattered H I Lα at $\rho \gtrsim 2R_\odot$ and to undertake measurements of other coronal parameters such as magnetic fields (Bommier and Sahal-Brechot, 1982). A detailed definition study of a UV/white light coronagraphic instrument package suitable for flight on Spacelab or Space Platform has been conducted (cf. Kohl *et al.*, 1981). NASA science working groups have proposed several missions in which UV/white light coronagraphs play an important role, the Solar Coronal Explorer (SCE), the Solar Terrestrial Observatory (STO) and the Pinhole/Occulter Facility (POF). The SCE has an instrument complement consisting of a white light coronagraph, UV/EUV coronagraph, soft X-ray imaging telescope and XUV spectrometer designed to study the corona over a period of several years from a spacecraft similar to SMM or a Space Platform (Orrall *et al.*, 1981). The STO (Canfield *et al.*, 1981) is an instrument package with two groups of experiments mounted on Shuttle-serviced orbiting platform. One group of instruments studies the solar radiative output and the corona as a source of solar wind, while the other group studies the response of the terrestrial atmosphere to variations in the radiative and particle flux from the Sun. The POF (Hudson *et al.*, 1981) employs an occulter on a 50 m boom (see Figure 14) which casts a large shadow permitting the use of large aperture (~ 1 m) coronagraphic instruments. The occulter also

© Kluwer Academic Publishers • Provided by the NASA Astrophysics Data System

1982SSRv...33...17W

Fig. 14. Illustration of the Pinhole/Occulter Facility (POF) with its 50 m boom deployed from the Orbiter bay. POF would provide a distant external occulter capable of shielding large aperture coronagraphic optics from bright solar disk radiation and also provide a pinhole array for high resolution imaging in hard X-ray radiation.

serves as a multi-pinhole array for high resolution ($\lesssim 1$ arc sec) hard X-ray imaging. Because of the large photon collecting capability of the POF coronagraphs, they can provide measurements with high spatial resolution (~ 1 arc sec, an order of magnitude or more better than more conventional instruments) and good time resolution for studying transient phenomena, as well as providing a capability for measuring weak coronal lines at large distances beyond the limb of the Sun.

12. Summary

Through use of the plasma diagnostic information contained in UV and EUV emission lines it is possible to greatly expand our knowledge about the physical conditions in the solar wind acceleration region $r \gtrsim 1.3 R_\odot$. Coronagraphic measurements of the intensities and profiles of the resonantly scattered and electron scattered components of hydrogen Lα coupled with measurements of the intensity and polarization of the electron scattered white light continuum can provide information on T_e, T_p, N_e, $N_{\mathrm{H\,I}}$, and outflow velocities greater than 100 km s^{-1}. A more complete description of

© Kluwer Academic Publishers • Provided by the NASA Astrophysics Data System

1982SSRv...33...17W

conditions in the upper corona is obtained when measurements of spectral lines from heavier ions are simultaneously measured with Lα to yield information on ion kinetic temperatures, non-thermal particle velocities, ion densities, chemical abundances and flow velocities in the range 30–100 km s^{-1}, plus additional constraints on T_e and N_e. The information provided by combined UV/EUV and white light observations is a considerable improvement over having only N_e obtained from traditional white light coronagraphs.

Plasma diagnostic information derived from spectroscopic measurements can provide critical empirical constraints on mechanisms for plasma heating, solar wind acceleration, and transport of mass, momentum and energy, as well as mechanisms responsible for producing differences in chemical composition in the solar wind acceleration region. Information on temperatures and flow velocities is particularly important for investigating plasma heating and solar wind acceleration mechanisms and separation of mechanisms that depend upon driving the solar wind thermally and those driving it through wave-particle interactions. In addition, empirical data obtained from optical measurements of the solar wind acceleration region can be related to *in situ* measurements of electron and ion temperatures, flow velocities, abundances, charge states, etc. made in the solar wind at large distances from the Sun. The overall goal is understanding the physical processes and mechanisms operating in the solar corona and inner heliosphere. This knowledge can advance our understanding of the physics of stellar coronae and stellar mass loss, as well as improving the understanding of solar wind physics and the physics of the interplanetary medium.

Acknowledgements

This work was supported by NASA under grants NSG 5128 to the Harvard College and NAGW–249 to the Smithsonian Institution and under Order No. W–13 998 to the High Altitude Observatory and by the Fluid Research Fund and Langley–Abbott Program of the Smithsonian Institution.

References

Ahmad, I. A.: 1977, *Solar Phys.* **53**, 409.

Allen, C. W.: 1963, *Astrophysical Quantities*, 2nd ed., University of London, Athlone Press.

Bame, S. J., Ashbridge, J. R., Feldman, W. C., and Kearney, P. D.: *Solar Phys.* **35**, 137.

Basri, G. S., Linsky, J. L., Bartoe, J. D. F., Brueckner, G. E., and Van Hoozier, M. E.: 1979, *Astrophys. J.* **230**, 924.

Beckers, J. M. and Chipman, E.: 1974, *Solar Phys.* **34**, 151.

Blackwell, D. E., DeWhirst, D. W., and Ingham, M. E.: 1967, *Astron. Astrophys.* **5**, 1.

Bommier, V. and Sahal-Brechot, S.: 1982, *Astron. Astrophys.*, in press.

Brueckner, G. E.: 1980, *Highlights of Astronomy* **5**, 557.

Canfield, R. C., Chappell, C. R., Eddy, J. A., Farmer, C. B., Fisk, L. A., Geller, M. A., Gosling, J. T., MacQueen, R. M., Nagy, A. F., Neugebauer, M. M., Paulikas, G. A., Russell, C. T., Russell, P. B., Tandberg-Hanssen, E. A., and Taylor, W. W. L.: 1981, *Solar Terrestrial Observatory*, Final Report of the Science Study Group, NASA Marshall Space Flight Center.

Cram, L. E.: 1976, *Solar Phys.* **48**, 3.

© Kluwer Academic Publishers • Provided by the NASA Astrophysics Data System

1982SSRv...33...17W

Cushman, G. W. and Rense, W. A.: 1976, *Astrophys. J.* **207**, L61.
Dupree, A. K. and Reeves, E. M.: 1971, *Astrophys. J.* **165**, 599.
Dupree, A. K., Huber, M. C. E., Noyes, R. W., Parkinson, W. H., Reeves, E. M., and Withbroe, G. L.: 1973, *Astrophys. J.* **182**, 321.
Feldman, U. and Behring, W. E.: 1974, *Astrophys. J.* **189**, L45.
Feldman, W. C., Asbridge, J. R., Bame, S. J., and Gosling, J. T.: 1977, in O. R. White (ed.), *The Solar Output and Its Variations*, Colorado Assoc. Univ. Press, p. 351.
Fite, W. L., Smith, A. C. H., and Stebbings, R. F.: 1962, *Proc. Roy. Soc. Ser. A* **268**, 527.
Gabriel, A. H.: 1971, *Solar Phys.* **21**, 392.
Gabriel, A. H., Garton, W. R. S., Goldberg, L., Jones, T. J. L., Jordan, C., Morgan, F. J., Nicholls, R. W., Parkinson, W. H., Paxton, H. J. B., Reeves, E. M., Shenton, D. B., Speer, R. J., and Wilson, R.: 1971, *Astrophys. J.* **169**, 595.
Gouttlebroze, P., Lemaire, P., Vial, J. C., and Artzner, G.: 1978, *Astrophys. J.* **225**, 655.
Hartle, R. E. and Sturrock, P. A.: 1968, *Astrophys. J.* **151**, 1155.
Henry, R. C., Anderson, R. C., and Fastie, W. G.: 1980, in I. Halliday and B. A. McIntosh (eds.), *Solid Particles in the Solar System*, D. Reidel Publ. Co., Dordrecht, Holland, p. 41.
Hirshberg, J.: 1975, *Rev. Geophys. Space Phys.* **13**, 1059.
Hollweg, J. V.: 1978, *Rev. Geophys. Space Phys.* **16**, 689.
Hollweg, J. V.: 1981, in S. Jordan (ed.), *The Sun as a Star*, NASA SP-450, NASA, Washington, D.C., p. 355.
Holzer, C. J. van: 1950, *Bull. Astron. Inst. Neth.* **11**, 160.
Hudson, H. S., Kohl, J. L., Lin, R. P., MacQueen, R. M., Tandberg-Hansen, E., and Dabbs, J. R.: 1981, *The Pinhole/Occulter Facility*, NASA Technical Memorandum NASA TM-82413, NASA, Marshall Space Flight Center, Alabama.
Hughes, C. J.: 1965, *Astrophys. J.* **142**, 321.
Hundhausen, A. J.: 1972, *Coronal Expansion and Solar Wind*, Springer-Verlag, New York.
Hyder, C. L. and Lites, B. W.: 1970, *Solar Phys.* **14**, 147.
Ingham, M. F.: 1961, *Monthly Notices Roy. Astron. Soc.* **122**, 157.
Joselyn, J. A. and Holzer, T. E.: 1978, *J. Geophys. Res.* **83**, 1019.
Kohl, J. L. and Withbroe, G. L.: 1982, *Astrophys. J.* **256**, 263.
Kohl, J. L., Reeves, E. M., and Kirkham, B.: 1978, in K. A. van der Hucht and G. Vaiana (eds.), *New Instrumentation for Space Astronomy*, Pergamon, New York, p. 91.
Kohl, J. L., Weiser, H., Withbroe, G. L., Noyes, R. W., Parkinson, W. H., Reeves, E. M., Munro, R. H., and MacQueen, R. M.: 1980, *Astrophys. J.* **241**, L117.
Kohl, J. L., Withbroe, G. L., Weiser, H., MacQueen, R. M., and Munro, R. H.: 1981, *Space Sci. Rev.* **29**, 419.
Kohl, J. L., Weiser, H., Parkinson, W. H., Withbroe, G. L., and Munro, R. H.: 1982, (in preparation).
Lillie, C. F.: 1972, in *The Scientific Results from the Orbiting Astronomical Observatory OAO-2*, NASA SP-310, p. 95.
Linert, C., Richter, I., Pitz, E., and Planck, B.: 1981, *Astron. Astrophys.* **103**, 177.
Mariska, J. T.: 1977, Ph.D. Thesis, Harvard University.
Moe, O. K. and Nicolas, K. R.: 1977, *Astrophys. J.* **211**, 579.
Munro, R. H. and Jackson, B. V.: 1977, *Astrophys. J.* **213**, 874.
Munro, R. H. and Mariska, J. T.: 1977, *Bull. Am. Astron. Soc.* **9**, 370.
Munro, R. H., Kohl, J. L., Weiser, H., and Withbroe, G. L.: 1982, (in preparation).
Nerney, S. and Barnes, S. A.: 1977, *J. Geophys. Res.* **62**, 3213.
Newkirk, G., Jr.: 1967, *Ann. Rev. Astron. Astrophys.* **5**, 213.
Newkirk, G., Dupree, R. G., and Schmahl, E. J.: 1970, *Solar Phys.* **15**, 15.
Orrall, F. Q. and Speer, R. J.: 1973, *Solar Phys.* **29**, 41.
Orrall, F. Q., Barnes, A., Burlaga, L. F., Kahler, S. W., Munro, R. H., Pneuman, G. W., Sheeley, N. R., Walker, A. B. C., and Withbroe, G. W.: 1981, *Solar Coronal Explorer*, Science Working Group Report, NASA Goddard Space Flight Center.
Owocki, S. P.: 1982, Ph.D. Thesis, U. Colorado.
Owocki, S. P. and Scudder, J.: 1982, submitted to *Astrophys. J.*
Percival, I. C.: 1966, *Nucl. Fusion* **6**, 182.
Perry, R. M. and Altschuler, M. D.: 1972, *Solar Phys.* **28**, 435.
Prinz, D. K.: 1974, *Astrophys. J.* **187**, 369.
Roser, S. and Staude, H. J.: 1978, *Astron. Astrophys.* **67**, 381.

© Kluwer Academic Publishers • Provided by the NASA Astrophysics Data System

1982SSRv...33...17W

Rottmann, G. J., Orrall, F. Q., and Klimchuk, J. A.: 1981, *Astrophys. J.* **247**, L135.
Rottmann, G. J., Orrall, F. Q., and Klimchuk, J. A.: 1982, submitted to *Astrophys. J.*
Saito, K.: 1970, *Ann. Tokyo Astron. Obs. Ser. 2* **12**, 53.
Spitzer, L., Jr.: 1962, *Physics of Fully Ionized Gases,* Interscience, New York.
Vaiana, G. S. and Rosner, R.: 1978, *Ann. Rev. Astron. Astrophys.* **16**, 393.
van de Hulst, H. C.: 1947, *Astrophys. J.* **105**, 471.
van de Hulst, H. C.: 1950, *Bull. Astron. Inst. Neth.* **11**, 135.
Vernazza, J. E. and Reeves, E. M.: 1978, *Astrophys. J. Suppl.* **37**, 485.
Weinberg, J. L. and Sparrow, J. G.: 1978, in McDonnell (ed.), *Cosmic Dust*, Wiley, New York, p. 75.
Weiser, H., Kohl, J. L., Parkinson, W. H., and Withbroe, G. L.: 1981, *Bull. Am. Astron Soc.* **12**, 917.
Wilson, D. C.: 1977, *The Three Dimensional Solar Corona – A Coronal Streamer, NCAR/CT-40*, Univ. of Colo. and Nat. Center Atmos. Res.
Withbroe, G. L.: 1970, *Solar Phys.* **11**, 42.
Withbroe, G. L. and Noyes, R. W.: 1977, *Ann. Rev. Astron. Astrophys.* **15**, 363.
Withbroe, G. L., Kohl, J. L., Weiser, H., Noci, G., and Munro, R. H.: 1982, *Astrophys. J.* **254**, 361.
Zirker, J. B.: 1981, in S. Jordan (ed.), *The Sun as a Star,* NASA SP-450, NASA, Washington, D.C.

© Kluwer Academic Publishers • Provided by the NASA Astrophysics Data System